NASA Contractor Report 172410

Flutter Parametric Studies Of Cantilevered Twin-Engine-Transport Type Wing With And Without Winglet

Volume I. Low-Speed Investigations

Kumar G. Bhatia, and K.S. Nagaraja

Boeing Commercial Airplane Company

Seattle, Wa.

Contract NAS1-17539

September 1984

National Aeronautics and Space Administration

Langley Research Center
Hampton Virginia 23665

FOREWORD

This document presents results of a recently completed joint Boeing-NASA program to study the effects of winglets on flutter characteristics of twin—engine transport type wings and to verify flutter analysis methodology. This document is one of the two proposed NASA publications dealing with this study and contains details sufficient to permit independent vibration and flutter analysis. A second publication, a NASA Technical Paper (TP), is planned for 1985, and will contain a technical summary. The present document is in two volumes:

Volume I - Low-Speed Investigations
Volume II - Transonic & Density Effect Investigations.

The two volumes are arranged such that each volume may be used independently of the other volume. The foreword and introduction are common to both volumes and are included in each volume along with a complete table of contents covering both volumes.

Mr. C. L. Ruhlin of Configuration Aeroelasticity Branch of NASA Langley Research Center was the test engineer for flutter tests conducted in the NASA Langley 16' Transonic Dynamic Tunnel, and was the contract monitor for preparation of the two NASA documents. The Boeing Commercial Airplane Company personnel who were major contributors to this study are:

K. G. Bhatia	Flutter - Principal Investigator
J. F. Bueno	Structures - Program Manager
A. W. Byrski	Loads & Flutter - Supervisor
W. F. Carver	Loads
M. G. Friend	Model Design
J. J. Hill	Weights
R. G. Kunkel	Model Shop
D. W. Lee, Jr.	Weights
D. J. Marzano	Flutter
J. E. Morrison	Loads
R. M. Nadreau	Structural Dynamics Laboratory
K. S. Nagaraja	Flutter
C. R. Pickrel	Structural Dynamics Laboratory
S. Ros	Loads
J. L. Stelma	Flutter
J. H. Thompson	Model Design

SYMBOLS

C_{n_α}	SECTIONAL LIFT-CURVE SLOPE COEFFICIENT PER DEGREE ANGLE OF ATTACK
C_{n_β}	SECTIONAL LIFT-CURVE SLOPE COEFFICIENT PER DEGREE OF SIDESLIP ANGLE
C_N	TOTAL LIFT COEFFICIENT
g	STRUCTURAL DAMPING
M	MACH NUMBER

LIST OF CONTENTS
VOLUME I-LOW-SPEED INVESTIGATIONS

LIST OF TABLES - VOLUME I

LIST OF FIGURES - VOLUME I

LIST OF FIGURES - VOLUME I (Cont'd)

LIST OF FIGURES - VOLUME I (Cont'd)

LIST OF FIGURES - VOLUME I (Cont'd)

LIST OF FIGURES – VOLUME I(Cont'd)

APPENDIX

LIST OF FIGURES – VOLUME I (Concluded)

LIST OF CONTENTS

VOLUME II – TRANSONIC & DENSITY EFFECT INVESTIGATIONS

LIST OF TABLES - VOLUME II

LIST OF FIGURES - VOLUME II

LIST OF FIGURES – VOLUME II (Cont'd)

LIST OF FIGURES – VOLUME II (Cont'd)

LIST OF FIGURES - VOLUME II (Concluded)

LIST OF FIGURES - VOLUME II (Cont'd)

LIST OF FIGURES – VOLUME II (Cont'd)

APPENDIX A MODEL GEOMETRY, MASS & STIFFNESS DATA

LIST OF FIGURES - VOLUME II (Cont'd)

APPENDIX B AERODYNAMIC DATA

LIST OF FIGURES - VOLUME II (Cont'd)

APPENDIX B AERODYNAMIC DATA

LIST OF FIGURES – VOLUME II (Concluded)

APPENDIX C VIBRATION FREQUENCIES & NODE LINES

1.0 Summary

Flutter characteristics of a cantilevered high aspect ratio wing with winglet were investigated. The configuration represented a current technology, twin-engine airplane. A low-speed and a high-speed model were used to evaluate compressibility effects through transonic Mach numbers and a wide range of mass-density ratios. The results of the investigation are described in two volumes of this NASA CR and summarized in a forthcoming NASA TP. The results from the low-speed flutter test and analysis-test correlation are included in this Volume 1.

Four distinct flutter modes were identified from the test. Flutter occurred in the same modes as predicted by the analysis. The analysis-test correlation is considered to be good, and the trends are consistent for all configurations. The effect of static load, on the winglet related flutter, was found to be rather insignificant. The variation in the static load was obtained by changing model angle of attack from -2° to +2° or yaw angle from -5° to +5°.

The test results are summarized in Figure 1, and occurrence of the four flutter modes in various configurations is shown. The results for the flutter speeds and mechanisms were insensitive to fuel in 0% to 75% fuel range. In figure 2 the percent deviation of analytical flutter speeds from the test speeds, is shown. The flutter mechanisms observed in the test were the same as predicted by the analysis.

The low-speed flutter mechanism was found to be amenable to the conventional flutter analysis techniques. Extra effort devoted to properly defining the geometric relationship between stiffness and mass properties did probably help in obtaining the degree of analysis-test correlation. In fact the pretest analysis was found satisfactory enough so that no major effort was expended after the test to improve the correlation.

2.0 Introduction

The interest in using wing-tip-mounted winglets to reduce drag for transport airplanes was stimulated by the work reported in Reference (1). One of the first applications of winglets was for the KC-135 airplane based on a potential drag reduction of about six percent estimated in Reference (2). The KC-135 Winglet Flight Research and Demonstration Program was formulated to design, fabricate and flight test a set of winglets to prove the drag reduction and other characteristics of the winglet concept.This program included a low-speed wind-tunnel flutter model test and a flight flutter test program (Ref. 3). The critical mode during flight flutter test was a 3.0 Hz low-damped mode occurring with a light fuel loading at 21,500 feet altitude and with zero degree cant angle and -4 degrees incidence winglets. Flight testing for this configuration was terminated at 370 KEAS, rather than the test goal of 395 KEAS, due to low damping (g = 0.015). The low damping obtained for this mode was not predicted by flutter analysis. The lack of correlation was judged to be due to limitations of current linearized aerodynamic theory and inability to represent transonic effects. Winglets have also been considered for the B-747 airplane as a part of the NASA Energy Efficient Transport Program (Ref. 4). Two flutter modes were obtained in the low-speed model test for the configuration with winglets. These flutter mechanisms were not present for the baseline configuration without winglets and were shown to result from winglet aerodynamics rather than mass effects. Flutter speeds for the configuration with winglets were significantly lower than the baseline configuration. It was suggested that the flutter mechanisms could be predicted by incorporating static-lift effects as with T-tail type flutter analysis.

A transonic flutter model study of a supercritical wing with winglet for an executive-jet-transport airplane (Ref. 5) reported a good analysis-test correlation . The winglet addition decreased flutter speed by seven percent, of which a five percent decrease was due to the wing-tip mass effect. Thus, there was no significant reduction in flutter speed due to winglet aerodynamics. Results of another application of winglets for the DC-10 airplane, under the NASA Energy Efficient Transport Program, were recently published (Refs 6 and 7). A low-speed flutter model test showed that the winglets had

generally detrimental effects on the flutter characteristics with small-to-moderate degradation in the basic wing flutter mode and a large degradation in a higher frequency wing flutter mode. During the flight test of the DC-10 airplane with winglets, 500 pounds of mass balance was installed in each wing tip to ensure adequate flutter margins for flight testing.

It appears from the available data that winglets generally caused degradation in flutter speed. The actual reduction in flutter speed varied with the configuration. The KC-135 flight test experience of encountering an unexpected low-damped mode highlighted the technical risk involved in flutter assessment of an airplane configuration with winglets. The only transonic wind-tunnel flutter test data available on a scaled airplane wing was for an executive-jet-transport wing which showed a small reduction in flutter speed due to addition of a winglet. These considerations led to a joint Boeing/NASA program to develop a flutter methodology for winglet configured wings. A typical, current technology, twin-engine transport wing was selected as the basis for the study. A test program was outlined as follows:

A. Pressure Model Test for Aerodynamic Data Base

B. Low-Speed Test
   - (i) Model Ground Vibration Test (GVT)
   - (ii) Flutter Test and Parametric Studies
   - (iii) Analysis-Test Correlation

C. Test in NASA Langley 16' Transonic Dynamics Tunnel (TDT)
   - (i) Retest of Low-Speed Flutter Model for Mass-Density Ratio Effects
   - (ii) Selection of High-Speed Model Configurations
   - (iii) High-Speed Model GVT
   - (iv) High-Speed Model Flutter Test
   - (v) Analysis-Test Correlation

Cantilevered wing models were used in all three tests. It was judged that once the wing-winglet interaction was adequately represented, the effect of body and empennage on flutter could be accounted for.

The pressure model test was designed to collect aerodynamic data for both loads and flutter analysis. Figure 3 shows the model installation in the Boeing Transonic Wind Tunnel (BTWT). Pressure data was collected for a Mach number-angle of attack grid for the following configurations:

A. (i) Clean wing with nominal tip
   (ii) Clean wing with winglet at 20° cant angle (outboard relative to the vertical)

B. (i) Wing with nacelle and nominal tip
   (ii) Wing with nacelle and (a) Winglet at 20° cant
   (b) Winglet at 10° cant
   (c) Winglet at 0° cant

C. Configurations described under B above but with the wing sweep angle increased by 5°

D. Configurations described under B but with the wing sweep angle decreased by 5°

The pressure data was reduced to sectional data. The wing sectional data was linearized with respect to angle of attack to obtain C_{n_α}, and corrected to remove the effect of the model wing flexibility. The wing sectional data was also linearized with respect to the wing sweep angle to obtain C_{n_β}, but was not corrected for the model flexibility effects. The winglet sectional data was similarly linearized without being corrected for the model flexibility. The linearized sectional data was used in the flutter analysis.

The choice of flutter test configurations and parameters was dictated by the task definition, viz., to develop flutter methodology. Therefore, the test was planned to obtain different kinds of flutter modes so that the winglet mass and aerodynamic effects could be separately identified for each of the flutter modes. The low-speed flutter test was designed with a larger number and a wider range of parameters taking advantage of the relative ease of atmospheric low-speed flutter testing compared to high-speed testing.

The high-speed flutter test was designed after establishing analysis-test correlation for the low-speed flutter test. Based on the knowledge derived from the low-speed flutter test, a reduced number of configurations and parameters were selected for testing in the high-speed tunnel. The low-speed flutter test was conducted at the General Dynamics, Convair Division, San Diego wind tunnel facility. The transonic test was conducted in the NASA Langley 16' Transonic Dynamics Tunnel (TDT). A schematic diagram of the wing and the wing tips tested, is shown in figure 4.

The low-speed model wing was of conventional, single-spar construction with wing sections perpendicular to the spar. The configurations for the low-speed flutter model test were:

A.	(i)	Clean wing (without nacelle)
	(ii)	Wing with winglet (without nacelle)
	(iii)	Wing with winglet mass simulator (without nacelle)
B.	(i)	Wing with nacelle
	(ii)	Wing with nacelle and winglet
	(iii)	Wing with nacelle and winglet mass simulator
C.	(i)	Wing with nacelle boom
	(ii)	Wing with nacelle boom and winglet
	(iii)	Wing with nacelle boom and winglet mass simulator

The winglet mass simulator was designed to represent winglet weight, center of gravity and inertia properties to help separate winglet inertia and aerodynamic effects. The results from configurations with nacelle boom were not used due to good correlation obtained for the configurations with nacelle.

The parameters varied were:

a. angle of attack,
b. model yaw angle,
c. wing fuel (0%, 50%, 75%, and 100%),

d. nacelle strut side bending frequency,

e. nacelle strut vertical bending frequency,

f. winglet/simulator cant angle (0°, 10°, 20° relative to the vertical), and

g. winglet/simulator stiffness.

The variation of angle of attack and yaw angle was included to evaluate the static-lift effects. The effect of nacelle side bending frequency was found to be small for the test configuration, and is not discussed further in this document.

The main objective of flutter testing in the NASA Langley TDT was to determine the effects of Mach number on flutter characteristics. However, the flutter points obtained in a variable density, transonic tunnel depend upon the mass-density ratio as well as the Mach effects. Therefore the low-speed model was retested in TDT to determine altitude or mass-density ratio effects at low speeds. Only two configurations, empty wing with nominal nacelle and with and without winglet, were tested. The analysis had shown a switch in flutter mode, from nacelle vertical bending to second wing bending, due to decrease in the mass-density ratio. To obtain the mode change in the tunnel, mass-density ratio was varied by testing the configuration with winglet in both air and freon. The strategy was to show that the mass-density ratio effects, for a winglet configured wing, could be predicted at low Mach numbers. The flutter correlation at higher Mach numbers could then be evaluated on the basis of compressibility and transonic effects. The high-speed model was tested in freon for a Mach range of about 0.6 to 0.91 and dynamic pressures up to 200 psf.

The high-speed model was constructed primarily of fiberglass sandwich components with ribs, spars, stringers and skin representing a modern transport wing. Wing fuel was simulated by water. The model was instrumented with 20 accelerometers, 23 pressure transducers in two chordwise arrays, and strain gages to monitor wing and winglet loads. The following configurations were selected for testing:

A. Wing with nacelle and nominal tip

B. Wing with nacelle and ballasted tip

C. Wing with nacelle and winglet

The ballasted tip configuration was selected to determine the effect of winglet weight separately from winglet aerodynamics. A winglet mass simulator similar to that used on the low-speed model, would have introduced unknown aerodynamic effects at high speeds. Therefore, the ballast weight was incorporated inside the wing contour resulting in a wing tip aerodynamically identical to the nominal tip. The test parameters selected were:

a. wing fuel (empty and full),
b. nacelle strut vertical bending frequency,
c. winglet cant angle (0° and 20° relative to the vertical), and
d. angle of attack.

Two nacelle strut vertical bending springs were used. The nominal strut vertical bending spring (nominal nacelle) and the softer strut vertical bending spring (soft nacelle) gave rise to different flutter characteristics due to differences in coupling of nacelle motion with inboard wing torsion. A series of high angle of attack runs, within the model load limits, was run to verify that there were no single-degree-of-freedom instabilities at transonic speeds.

This volume pertains to the low-speed flutter test conducted in the Convair tunnel. The highlights are covered in the main body. The Appendix contains sufficient data, in the form of figures and tables, to allow an independent analysis. The vibration frequencies and node lines are also included in the Appendix.

3.0 Description of Test

Figure 5 shows the model setup in the wind tunnel with the Fourier Analyzer System (HP5451), Digital Signal Analyzer System (HP5420A) and the remote display (HP1311B) system. The right wing was mounted on a stiffened body, which was supported by a pitch mechanism to vary the angle of attack. The pitch mechanism in turn was mounted on an A-frame bolted to the tunnel balance such that the complete model assembly could be

yawed in the tunnel. Figure A1 (appendix) shows the wing, nacelle and winglet geometry. The wing sections, the nacelle installation and the body sections used were obtained from an existing model. A new wing spar, a nacelle boom simulating the nacelle c.g. location and inertia about the spar, a winglet, a winglet mass simulator and related winglet/simulator hardware were built. The winglet aerodynamic design was verified in the wind tunnel, and the winglet strength, mass properties and stiffness were calculated. Figures A2-A6 (appendix) describe the data defining the model.

The winglet/simulator stiffness variation was achieved by changing the spring supporting the winglet/simulator from the wing tip. A vibration analysis of the winglet supported at the wing tip (winglet root) was performed to determine the nominal winglet bending frequency of about 30.0 Hz. Based on this, 3 winglet frequencies were obtained: nominal (30.1 Hz), soft (21.8 HZ) and stiff (49.3 Hz). Similarly the simulator frequencies obtained were: nominal (28.1 Hz), soft (21.1 Hz) and stiff (52.1 Hz).

The winglet (simulator) with 20 degree cant and frequency of 30.1 Hz (28.1 Hz) was designated as nominal. Also, the nacelle strut vertical bending spring T20 and side bending spring S15 corresponding to cantilevered nacelle vertical bending frequency of 11.72 Hz and nacelle side bending frequency of 8.15 Hz, respectively, were designated as nominal. The configuration with nacelle vertical bending spring corresponding to cantilevered frequency of 8.79 Hz, was designated as soft nacelle.

4.0 Model GVT

A model GVT was conducted prior to the test. The GVT frequencies and mode shapes were compared to the analytical predictions. A good correlation between the analysis and test results was obtained. The frequency correlation for a few of the configurations is shown in Tables 1-4. Figures A7a-A7i (appendix) show the calculated node lines and frequencies for several configurations. The node lines from model GVT are shown for comparison, where available. Because of the degree of correlation achieved, no major tuning of the structural model was attempted.

Modal damping for the model was determined from the GVT. Structural damping for the modes expected to flutter was about .005, except for the nacelle vertical bending mode. The nacelle vertical bending mode had structural damping of about .015.

5.0 Test Results

The test data was carefully reviewed to establish description of the flutter modes encountered during the test. These descriptions were derived from oscillograph traces of the selected accelerometer responses and the "Cascade Plots" showing auto spectra of the wing tip vertical accelerometers through the test speed range for each run. In addition, the observations recorded in the test log and the movies taken during the test were used for corroboration of these descriptions. The flutter modes were categorized as follows:

a) Basic nacelle vertical bending mode (NVB mode) was characterized by relatively large nacelle and wing tip vertical motions. The nacelle motion led the wing tip generally by about 200°-270°. The flutter frequency of this mode was in the range of 8.3- 8.7 Hz except for runs with 100% fuel where this mode, when it occurred, had a frequency of 6.6–6.7 Hz.

b) Wing tip mode (WT mode) was characterized by high frequency and sudden flutter onset. It was a classic type of flutter mode where the wing bending and first torsion modes coalesce into a mode with rapidly reducing damping level and frequency. Therefore the flutter frequency for this mode depended upon the level of response at which the tunnel was stopped. When encountered for the clean wing configuration, the frequency recorded ranged from 12 to 22 Hz. For configurations with nacelle or nacelle and winglet, the frequency was approximately 14 Hz. The oscillograph traces for the 14 Hz mode showed wing tip chordwise motion almost in phase with wing tip vertical motion.

c) Second wing bending mode (WB2 mode) occurred only with winglet or simulator for certain fuel and nacelle vertical bending combinations. It was characterized by flutter frequency in the 10- 12 Hz range. With the winglet, the wing tip chordwise

motion led the wing tip vertical motion by about 200°. The wing tip chordwise motion was seen to be distinctly harmonic and of similar amplitude as the wing tip vertical for the winglet configurations. For simulator configurations, the wing tip chordwise motion was not evident.

d) Combination wing chordwise and tip mode (WCT mode) was characterized by prominence of 10.0 Hz wing chordwise mode along with higher wing frequency mode of about 14-15 Hz (in the auto spectra from the wing tip vertical accelerometer). In the oscillograph traces, the wing tip chordwise motion led the wing tip vertical motion by about 250° or the two were almost in phase. For several runs, it appeared that the chordwise motion first increased with speed, then decreased, before the tunnel was shut down due to the wing tip vertical response. This flutter mode appeared only for the 100% fuel condition.

The flutter test results have been plotted with respect to various parameters and a summary is included as Figures 6a to 6f. The test runs were terminated when there was excessive model amplitude due to flutter. Two accelerometers monitoring wing tip and nacelle vertical responses were connected to a Boeing designed Dynamic Response Actuation System (DRAS) such that acceleration amplitudes above a preset level caused automatic tunnel shutdown.

(i) Wing without nacelle: Figures 6a and 6b show the variation of flutter speed versus percent fuel. The clean wing flutter mode was the hard wing tip (WT) mode. The flutter speed was not sensitive to the wing fuel and was around 124 KTAS. Addition of the winglet mass simulator or the winglet changed the flutter mechanism. For the 0%, 50%, and 75% fuels, the flutter mode changed to second wing bending (WB2) mode. For the 100% fuel the flutter mode changed to the combination wing chordwise and tip (WCT) mode. The effect of the tip weight was to reduce the flutter speed by about 3% for the partial fuels and to increase by about 4% for the 100% fuel. The winglet aerodynamic effect as shown by difference between the simulator and winglet flutter speeds in Figure 6b, was significant. Flutter speeds for the WB2 and WCT modes dropped by about 19% and 26%, respectively, due to the winglet aerodynamic effects.

(ii) Wing with nacelle: Figures 6c and 6d show the variation of flutter speed versus percent fuel for two nacelle vertical bending frequencies. The higher frequency nacelle vertical bending strut (11.72 Hz) caused flutter to occur in the basic nacelle vertical bending (NVB) mode for all fuels. With the lower frequency nacelle vertical bending strut (8.79 Hz), the NVB mode occurred only for the 100% fuel while the flutter mode for the partial fuels was the hard wing tip (WT) mode.

(iii) Wing with nacelle and winglet or simulator: Figures 6e and 6f show the effect of winglet as well as simulator for the two nacelle vertical bending frequencies.

Flutter characteristics for the three partial fuel cases were similar to each other and the flutter speeds were within 3 KTAS of each other. The flutter characteristics for the partial fuel cases were different from the full fuel case. For the partial fuel with nominal nacelle, the flutter mode remained as the basic NVB mode. The flutter speed with the simulator tip increased by about 6% over the nominal tip. But with the winglet tip, the flutter speed decreased by about 13% relative to flutter speed with the simulator tip. For the soft nacelle configuration, flutter mode changed from the WT mode for nominal tip to the WB2 mode for simulator and winglet tips. The flutter speed with the simulator tip decreased by about 5% relative to the nominal tip. The winglet tip reduced the flutter speed by about 19% relative to the simulator tip.

For the full fuel with either nominal or soft nacelle, flutter occurred in the basic NVB mode at about the same speed for both the nominal and simulator wing tips. However, the flutter mode changed to the WT mode for the winglet tip, and the speed was lower by about 7% relative to the simulator tip.

In all cases the winglet effect was to significantly reduce the flutter speed. The winglet mass effect was to either increase or slightly decrease the flutter speed. Hence winglet aerodynamics was the major contributor to the reduction in flutter speed.

The effect of cant angle for the simulator configurations was not very significant in the range of cant angles tested (0 to 20°). However for the winglet configurations, increasing the cant angle reduced the flutter speeds as shown in figures 7a to 7d. The reduction appeared to be more pronounced for the 100% fuel than for the 75% fuel. The primary effect was due to the winglet aerodynamics. It appears that the flutter speeds would be minimum for a cant angle that would make the winglet as if it were a wing tip extension.

Effect of nacelle vertical bending frequency on flutter speed is shown in figures 8a - 8d. Two flutter modes - wing tip (WT) and nacelle vertical bending (NVB) - were obtained for the wing with 75% fuel and nominal tip (figure 8a). The effect of nacelle vertical bending frequency for the wing with 75% fuel and simulator or winglet tip, is shown in figure 8b. At the lower nacelle vertical bending frequency, flutter occurred in the second wing bending (WB2) mode. For the full fuel cases (figs 8c and 8d), there was no change in flutter mode due to the nacelle vertical bending frequency.

The flutter speeds did not exhibit sensitivity to winglet/simulator frequency. For some simulator configurations, the soft spring frequency caused automatic tunnel shutoff to trip due to a 19-20 Hz mode. This mode involved coupling between the nacelle roll and simulator bending. For one of the configurations, addition of an aerodynamically contoured shroud over the simulator caused the flutter to occur in the lower frequency mode. This indicates that the high frequency mode may have been excited due to the effect of the "dirty" aerodynamic configuration of the simulator.

Figures 9a and 9b show the effect of pitch and yaw angle variations on the flutter characteristics of the wing-nacelle, wing-nacelle-simulator, and wing-nacelle-winglet configurations. It is seen that the effect of static lift on the flutter speeds was relatively insignificant. The small variations in the flutter speeds can not, however, be attributed to data scatter since the repeatability of the flutter speeds (with DRAS) appeared to be within about 1 KTAS.

6.0 Flutter Analysis

The model was analysed using conventional flutter analysis techniques. The model spar was represented by finite beam elements (elastic axis). The nacelle and strut were attached as rigid, lump-masses to the wing elastic axis. The winglet and ballasted tip were represented as separate substructures using branch mode representation. The cantilevered nacelle strut and winglet test frequencies and mode shapes were input as assumed modes. The calibrated model stiffness properties were incorporated to improve correlation with the results of the model GVT. The aerodynamic representation for flutter analysis was based on the strip theory aerodynamics using fourteen wing strips. The sectional, static aerodynamics data was derived from wind-tunnel pressure tests. It was recognized that the spatial relation between the wing spar and the weights distribution must be properly defined. This is important for all flutter analyses, but is even more important when a significant weight is added at the tip. Therefore, the spar geometry was defined using the sweep, dihedral and side-of-body incidence to correctly locate the wing section attachments. The section weights data obtained were input relative to the section attachments. The modeling was done using the current version of the ATLAS program (Ref. 8), and the flutter analysis was conducted using the AF1 Aerodynamics program (unsteady, lifting line theory).

The pretest analysis predicted the four flutter modes, described in Section 5.0, for appropriate configurations. The analytical flutter speed trends generally agreed with trends from the test. Figures 10a through 10e show a comparison of the flutter speeds for the wing, wing-nacelle, wing-nacelle-simulator and wing-nacelle-winglet configurations. The flutter speeds for NVB mode are plotted for structural damping (g) of 0.015; speeds for rest of the modes is for g = 0.005. These damping values are in accordance with the model GVT results. The wing chordwise bending mode appeared as a low-damped flutter mode, for some configurations, in the analysis, and retained its low-damped character at least until another mode such as wing tip mode became unstable. Because of the low-damped characteristics of the wing chordwise mode, it can be expected not to show up as an unstable mode in the tunnel. However, the flutter in the wing tip mode can be expected to occur with significant wing chordwise motion. This was seen distinctly for the 100% fuel case for wing (100% fuel) - nacelle (soft) - winglet (nominal) configuration (fig. 10.e) where the test flutter mode was identified as a WCT mode. For the wing

(100% fuel)- nacelle (nominal) -winglet(nominal) case, fig 10-c, the test flutter mode did not seem to have significant chordwise motion as would be expected from the analytical prediction. The reason for this was not thoroughly investigated. Figures 10f and 10g compare the analysis and test results for winglet cant angle variation for 75% fuel condition. It is seen that the analysis-test correlation for the winglet variations is reasonably good, and consistent with analysis-test correlation for conventional wings without winglets. The analysis correctly predicted the effect of simulator or winglet on the flutter speed, and also predicted the correct flutter modes.

The analytical flutter speeds were generally somewhat higher than the test flutter speeds. The surprising aspect of the correlation has been that for most cases, the best match has been for the configurations with winglet. It was determined that the analysis-test correlation could be improved by making the following changes to the pretest analytical model:

a) interpolating the vibration modes in a streamwise direction rather than in a direction perpendicular to the elastic axis,

b) modifying the low speed sectional wing C_{n_α} distribution to improve the representation of pressure peak near the wing leading edge.

The above changes were incorporated in the model analysis and flutter speeds were calculated for various nacelle vertical bending frequencies for 0%, 75% and 100% fuel conditions. A comparison of analysis and test for these variations is shown in figures 11a, 11b and 11c. It appears that the analysis-test correlation for the nacelle vertical bending made, is better at g = .02 rather than g = .015. In the analysis for the empty fuel case, flutter speed for the second wing bending mode is higher than the test flutter speed by about 5%. The correlation for 75% fuel case is good. For the 100% fuel case the analytically predicted, low-damped wing chordwise bending mode appeared in the test as a 10 Hz model chordwise response. The analytical flutter speeds for the wing tip mode are again about 5% lower than the test speeds. It is believed that there is room for improvement in the analytical structural modeling. However, a reduction of analysis-test flutter speed correlation to less than 5% was not a sufficient motivation to expend the necessary effort.

The effect of static lift on flutter speeds has been investigated using the method of Reference 9, incorporated in the current version of ATLAS. It was determined that the static lift does not significantly affect the flutter results. Based on the correlation obtained thus far, it is likely that the static deformation would also not have a significant effect.

7.0 Some Design Considerations for the Winglets

In order to determine the relative effects of the winglet weight, cg location and aerodynamics, an analytical parametric variation was done. The results are plotted in Figures 12a, 12b, and 12c. Figure 12a shows that for the configuration with winglet simulator, the fore-aft position of the cg is significant. The effect of tip weight (Figure 12b) was to increase the flutter speed up to a certain level. Increasing the weight beyond a certain point had very small effect. The weight effect is much less significant for the winglet case as shown in Figure 12c. The primary influence on flutter appears to be from the winglet aerodynamics. In a separate analysis, results not plotted here, the wing sectional C_{n_α} distribution was matched to the case where winglet is present but the winglet itself was not included. It was found that the flutter speed for the NVB mode dropped only by about 3 KTAS. This suggests that the primary reason for reduction in the flutter speed is the winglet aerodynamic force distribution on the winglet.

8.0 Conclusions and Recommendations

1. Model GVT results showed good correlation with analytically predicted frequencies and modes.

2. The low-speed flutter test was successfully conducted and good quality data were obtained.

3. The flutter modes, frequencies and speeds agreed well with the analytical results. The configurations with winglet have the same degree of test-analysis correlation as those without winglets.

4. The static lift effects did not significantly affect the flutter test results. This was also apparent from the analytical results.

9.0 References

1) Whitcomb,R.T., "A Design Approach and Selected Wind-Tunnel Results at High Subsonic Speeds for Wing-Tip Mounted Winglets," NASA TND-8260, July 1976.

2) Ishimitsu, K.K., "Aerodynamic Design and Analysis of Winglets," AIAA Paper 76-940, September 1976.

3) Kehoe, M.W., "KC-135 Winglet Program Review", NASA CP2211, 1982.

4) Boeing Company, "Selected Advanced Aerodynamics and Active Controls Technology Concept Development on a Derivative B-747 Aircraft," NASA CR 3164, February 1980.

5) Ruhlin, C.L.; Rauch, F.J.; and Waters, C., "Transonic Flutter Model Study of a Supercritical Wing and Winglet," J. Aircraft, Vol. 20, No. 8, August 1983.

6) Schollenberger, C.A.; Humphreys, J.W.; Heiberger, F.S.; and Pearson, R.M., "Results of Winglet Development Studies for DC-10 Derivatives," NASA CR 3677, March 1983.

7) Douglas Aircraft Company, "DC-10 Winglet Flight Evaluation" NASA CR 3704, June 1983.

8) Dreisbach, R.L. (Editor), "ATLAS - An Integrated Structural Analysis and Design System, ATLAS User's Guide," NASA CR-159041, 1979.

9) Jennings, W.B.; and Berry, M.A., "Effect of Stabilizer Dihedral and Static Lift on T-Tail Flutter," J. Aircraft, Vol. 14, No. 4, April 1977.

TABLE 1: CORRELATION OF ANALYSIS AND TEST VIBRATION FREQUENCIES (Hz) FOR CLEAN WING

(a) 0% FUEL

MODE	TEST	ANALYSIS
1st Wing Bending	4.51	4.55
1st Wing Chordwise Bending	--	14.18
2nd Wing Bending	14.99	15.07
1st Wing Torsion	29.25	30.35
3rd Wing Bending	33.93	35.10
2nd Wing Chordwise Bending	44.63	43.56
2nd Wing Torsion	45.29	49.12

(b) 75% FUEL

MODE	TEST	ANALYSIS
1st Wing Bending	4.49	4.43
2nd Wing Bending	12.51	12.43
1st Wing Chordwise Bending	--	13.48
3rd Wing Bending	25.78	26.12
1st Wing Torsion	28.49	28.64
2nd Wing Chordwise Bending	--	36.13
2nd Wing Torsion	41.32	43.65

(c) 100% FUEL

MODE	TEST	ANALYSIS
1st Wing Bending	3.46	3.45
1st Wing Chordwise Bending	-	10.40
2nd Wing Bending	10.59	10.51
3rd Wing Bending	21.74	21.77
1st Wing Torsion	25.12	25.15
2nd Wing Chordwise Bending	32.24	31.95
Higher Mode	33.66	39.19
Higher Mode	36.83	-
Higher Mode	41.81	43.44

TABLE 2: CORRELATION OF ANALYSIS AND TEST VIBRATION FREQUENCIES (Hz) FOR WING - NACELLE (NOMINAL)

NOMINAL NAC: S15/T20

75% FUEL

MODE	TEST	ANALYSIS
1st Wing Bending	4.42	4.42
Nacelle Side Bending	7.96	7.85
Nacelle Vertical Bending	9.49	9.12
2nd Wing Bending	12.44	12.44
1st Wing Chordwise Bending	14.07	13.55
Nacelle Roll	---	17.95
3rd Wing Bending	24.68	25.24
1st Wing Torsion	28.91	29.56
2nd Wing Chordwise Bending	36.22	34.89
Higher Mode	41.89	44.59

0% FUEL

MODE		ANALYSIS
1st Wing Bending	Test	4.53
Nacelle Side Bending	Data	7.87
Nacelle Vertical Bending	Not	9.16
1st Wing Chordwise Bending	Available	14.18
2nd Wing Bending		14.96
Nacelle Roll		17.98
3rd Wing Bending		31.15
Wing Torsion		31.60

TABLE 3: CORRELATION OF ANALYSIS AND TEST VIBRATION FREQUENCIES (Hz) FOR WING - NACELLE (NOMINAL) - SIMULATOR (NOMINAL)

(a) 0% FUEL

MODE	TEST	ANALYSIS
1st Wing Bending	3.93	3.77
Nacelle Side Bending	8.01	7 83
Nacelle Vertical Bending	9.30	9.13
1st Wing Chordwise Bending	12.30	11.70
2nd Wing Bending	12.73	11.95
Nacelle Roll	--	17.88
Wing Chordwise and 3rd Bending	23.51	23.47
Wing Torsion and Chordwise Bending	25.83	25.42
1st Wing Torsion	31.20	31.59
3rd Wing Bending	36.70	35.65
Higher Mode	42.97	43.84

(b) 75% FUEL

MODE	TEST	ANALYSIS
1st Wing Bending	3.91	3.71
Nacelle Side Bending	8.23	7.79
Nacelle Vertical Bending	9.38	9.08
2nd Wing Bending	10.80	10.47
1st Wing Chordwise Bending	12.53	11.50
Nacelle Roll	--	17.85
3rd Wing Bending	20.10	19.91
Wing Torsion and Chordwise Bending	24.40	24.00
1st Wing Torsion	28.50	28.72
Wing Chordwise and 3rd Wing Bending	31.90	31.06
2nd Wing Torsion	39.90	39.15

TABLE 4: CORRELATION OF ANALYSIS AND TEST VIBRATION FREQUENCIES (Hz) FOR WING - NACELLE (NOMINAL) - WINGLET (NOMINAL)

(a) 0% FUEL

MODE	TEST	ANALYSIS
1st Wing Bending	3.93	3.78
Nacelle Side Bending	--	7.83
Nacelle Vertical Bending	9.45	9.13
1st Wing Chordwise Bending	13.49	11.74
2nd Wing Bending	12.49	11.93
Nacelle Roll	--	17.88
Wing Chordwise Bending and Tip Torsion	23.46	22.85
Wing Torsion and Chordwise Bending	24.17	23.80
1st Wing Torsion	27.00	31.73
3rd Wing Bending	35.25	35.21
2nd Wing Torsion	42.14	40.82

(b) 75% FUEL

MODE	TEST	ANALYSIS
1st Wing Bending	3.90	3.72
Nacelle Side Bending	7.91	7.79
Nacelle Vertical Bending	9.51	9.08
2nd Wing Bending	10.70	10.47
1st Wing Chordwise Bending	12.30	11.52
Nacelle Roll	--	17.85
3rd Wing Bending	20.30	19.83
Wing Torsion and Chordwise Bending	23.30	22.46
1st Wing Torsion	28.50	28.45
Wing Chordwise and 3rd Wing Bending	31.40	30.66
2nd Wing Torsion	38.50	36.94

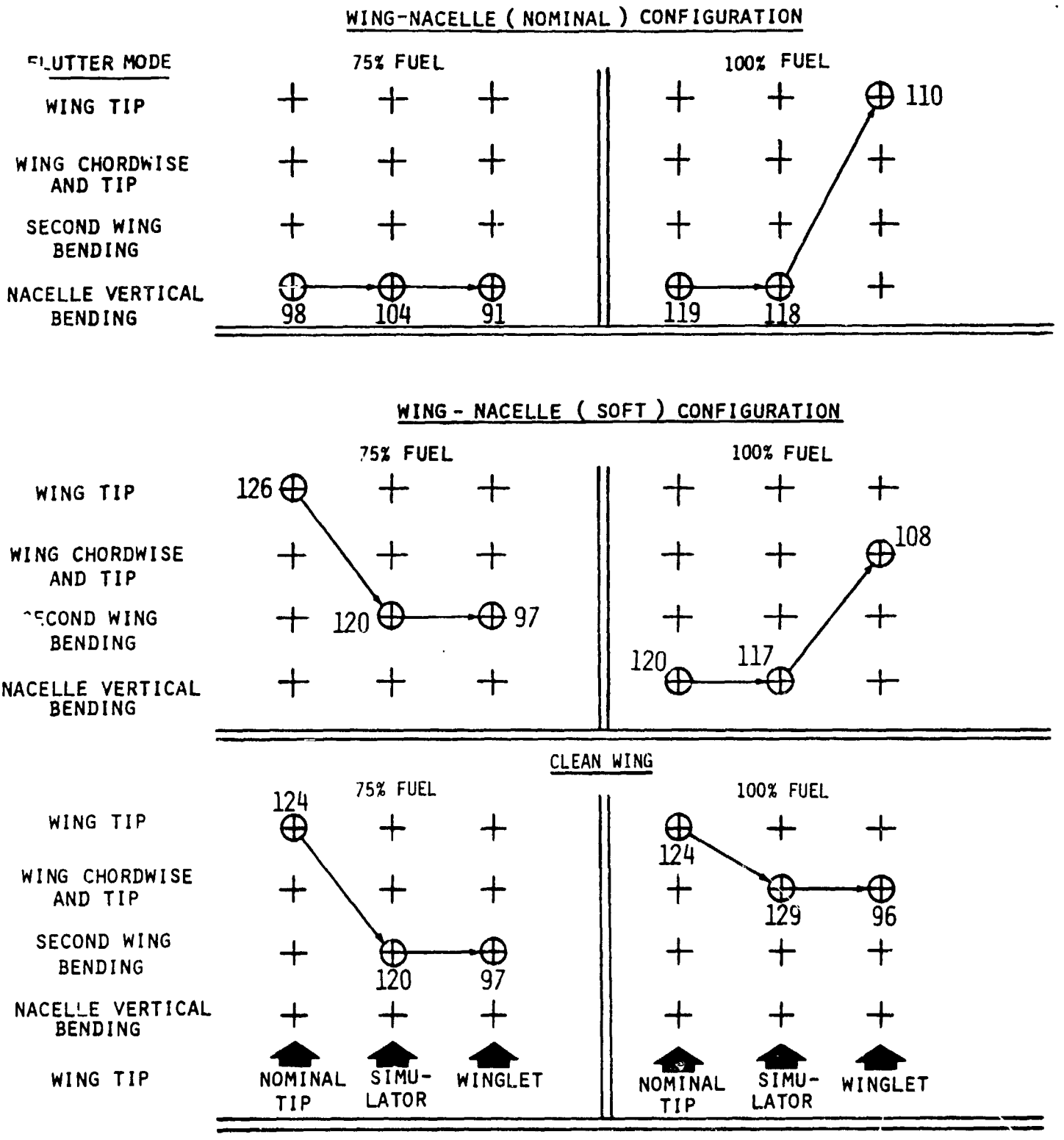

NOTE: (a) NUMBERS INDICATE TEST FLUTTER SPEEDS IN KTAS.

(b) NACELLE (NOMINAL) - 11.72 HZ. } NACELLE STRUT VERTICAL
NACELLE(SOFT) - 8.79 HZ. } BENDING FREQUENCY

FIGURE 1 SUMMARY OF LOW-SPEED FLUTTER TEST RESULTS

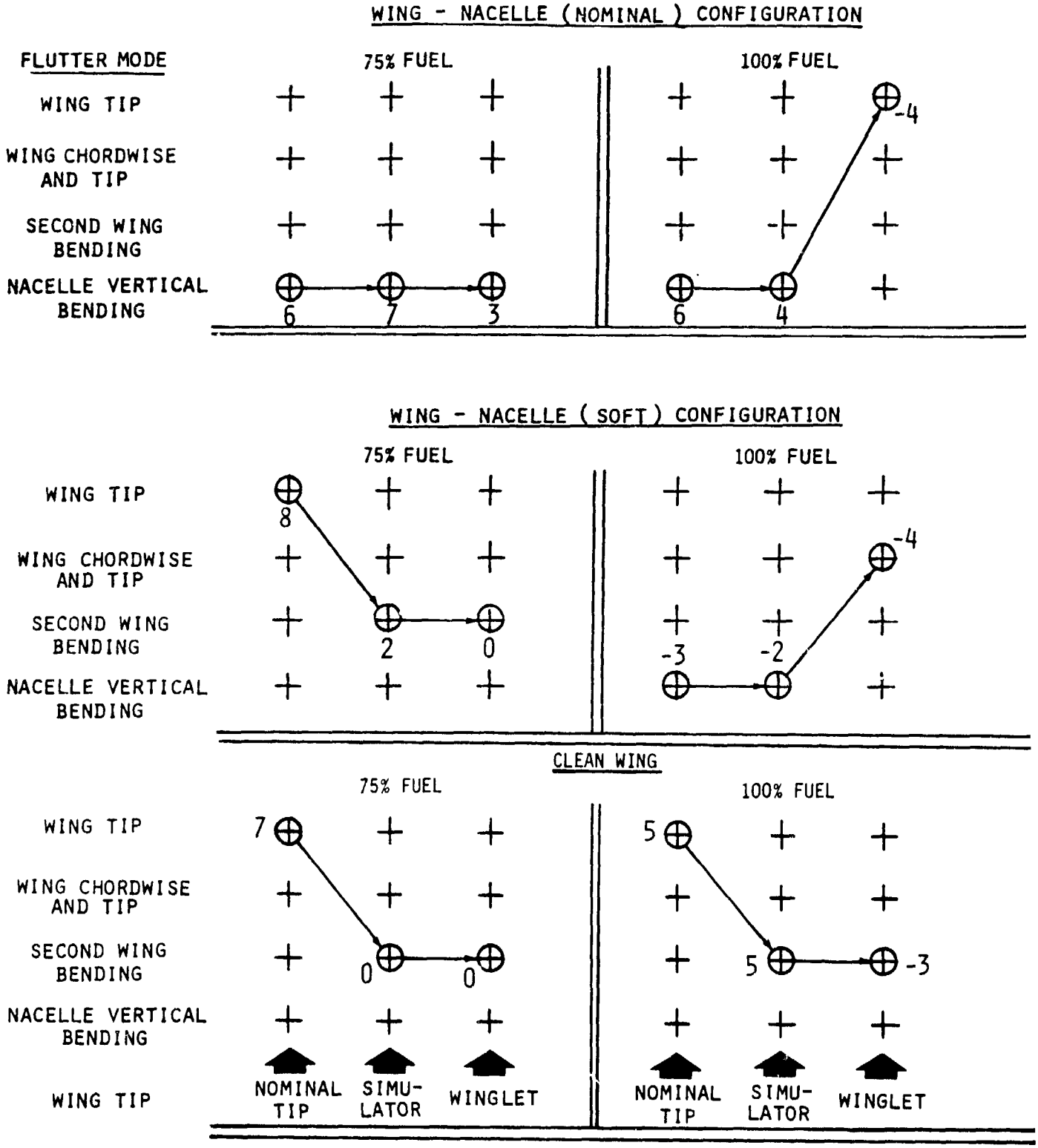

NOTE: (a) NUMBERS INDICATE PERCENT DEVIATION OF PREDICTED(ANALYSIS) FLUTTER SPEEDS FROM TEST FLUTTER SPEEDS

(b) NACELLE NOMINAL -11.72 HZ. } NACELLE STRUT VERTICAL
NACELLE(SOFT) -8.79 HZ. } BENDING FREQUENCY

FIGURE 2 SUMMARY OF LOW-SPEED TEST-ANALYSIS CORRELATION

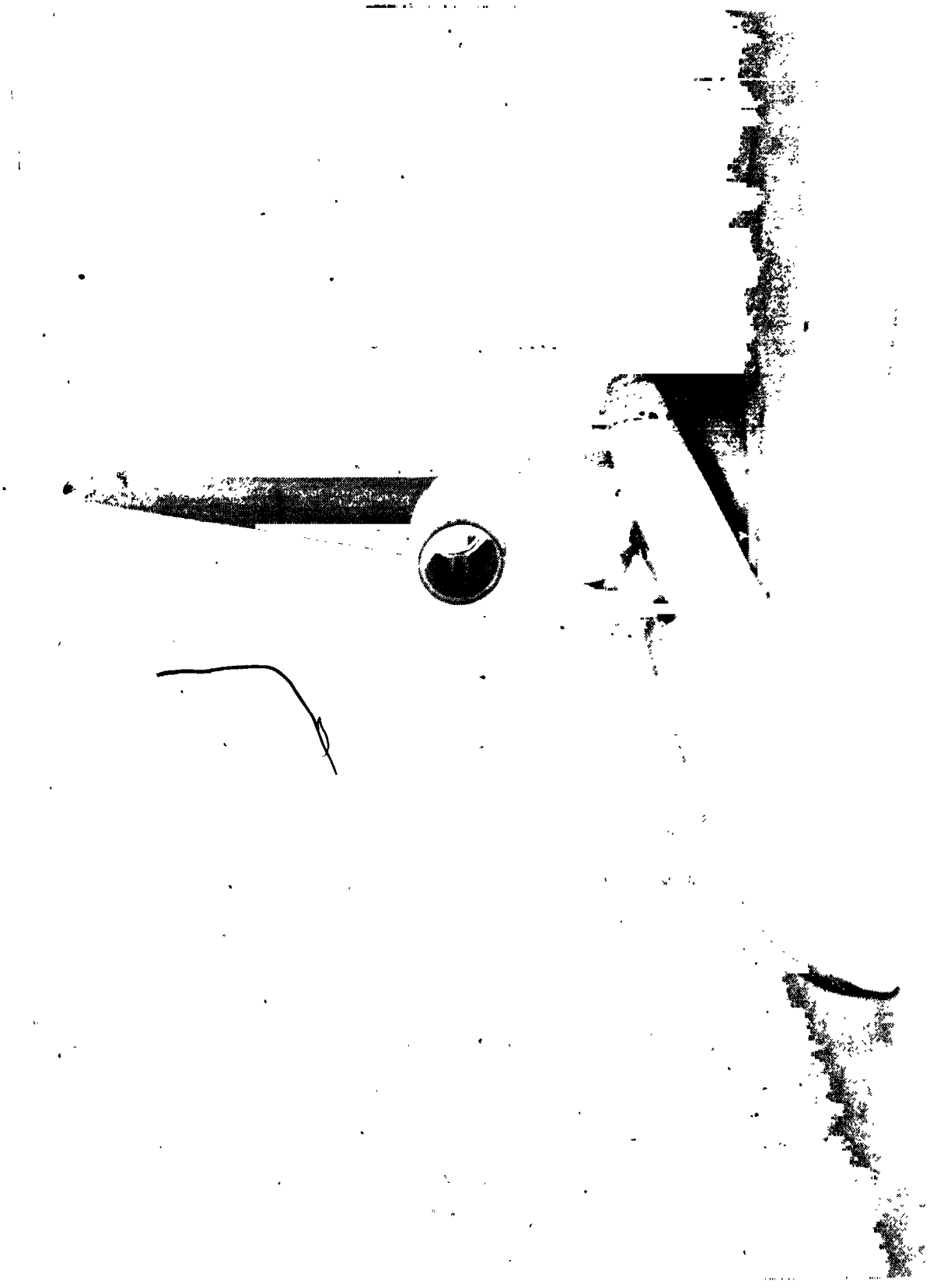

FIGURE 2 PRESSURE MODEL INSTALLATION IN BOEING TRANSONIC WIND TUNNEL

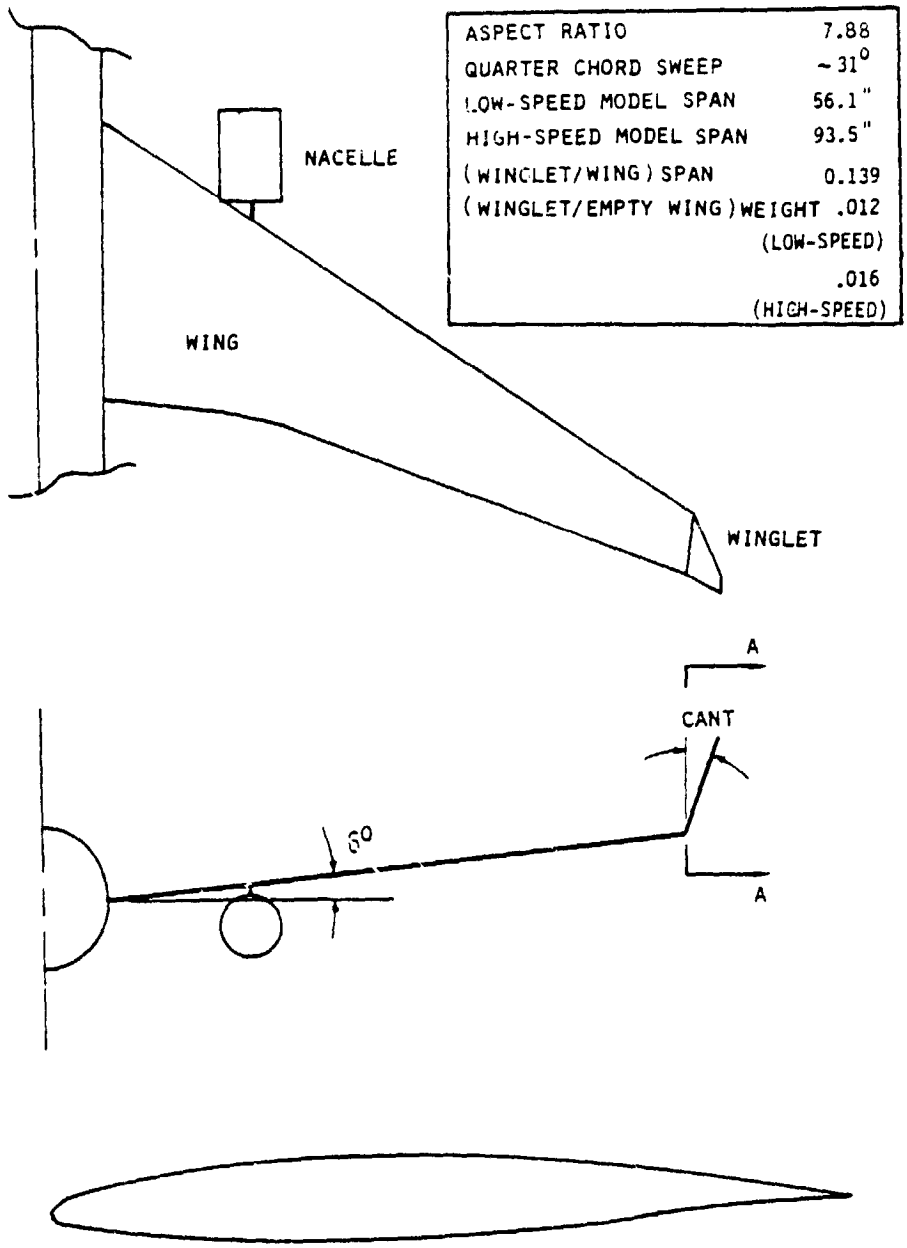

ASPECT RATIO	7.88
QUARTER CHORD SWEEP	~31°
LOW-SPEED MODEL SPAN	56.1"
HIGH-SPEED MODEL SPAN	93.5"
(WINGLET/WING) SPAN	0.139
(WINGLET/EMPTY WING) WEIGHT	.012 (LOW-SPEED)
	.016 (HIGH-SPEED)

TYPICAL MODEL WING SECTION

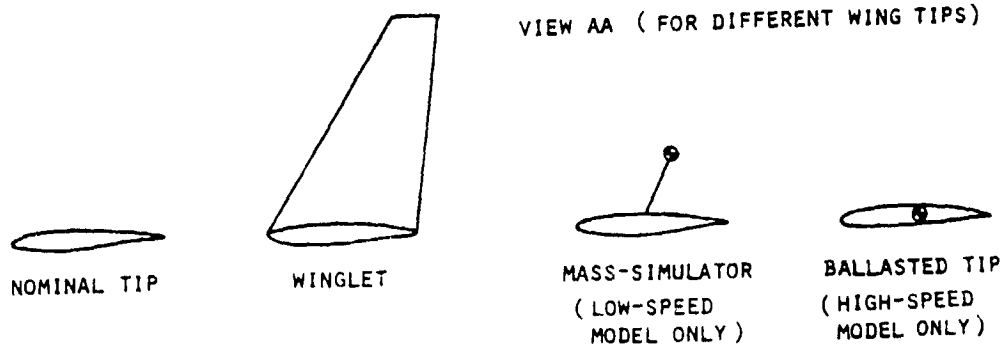

FIG. 4 MODEL WING AND WING TIPS

FIGURE 5 LOW-SPEED MODEL SET-UP IN THE CONVAIR TUNNEL

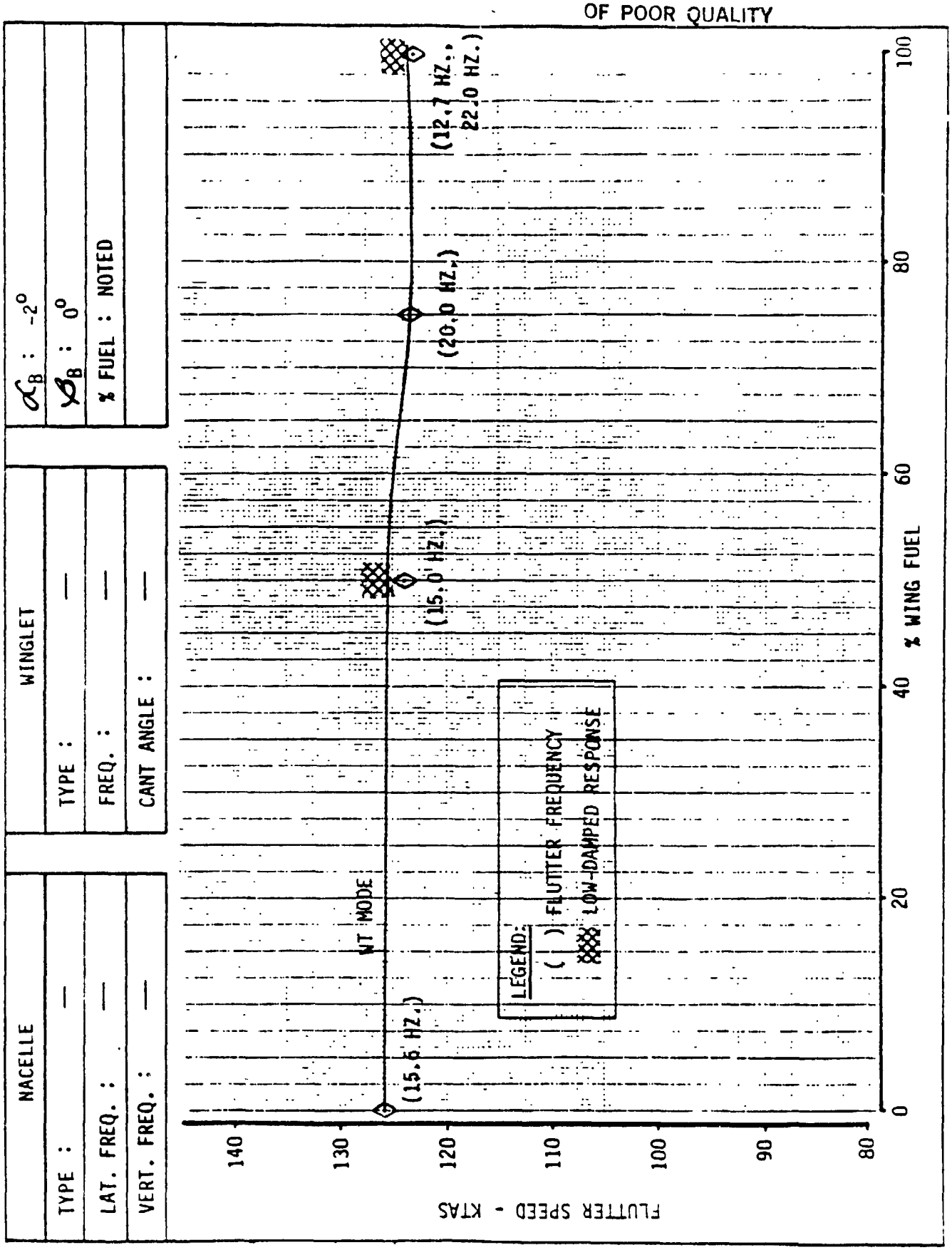

FIGURE 6a TEST FLUTTER SPEEDS VS. PERCENT FUEL, CLEAN WING

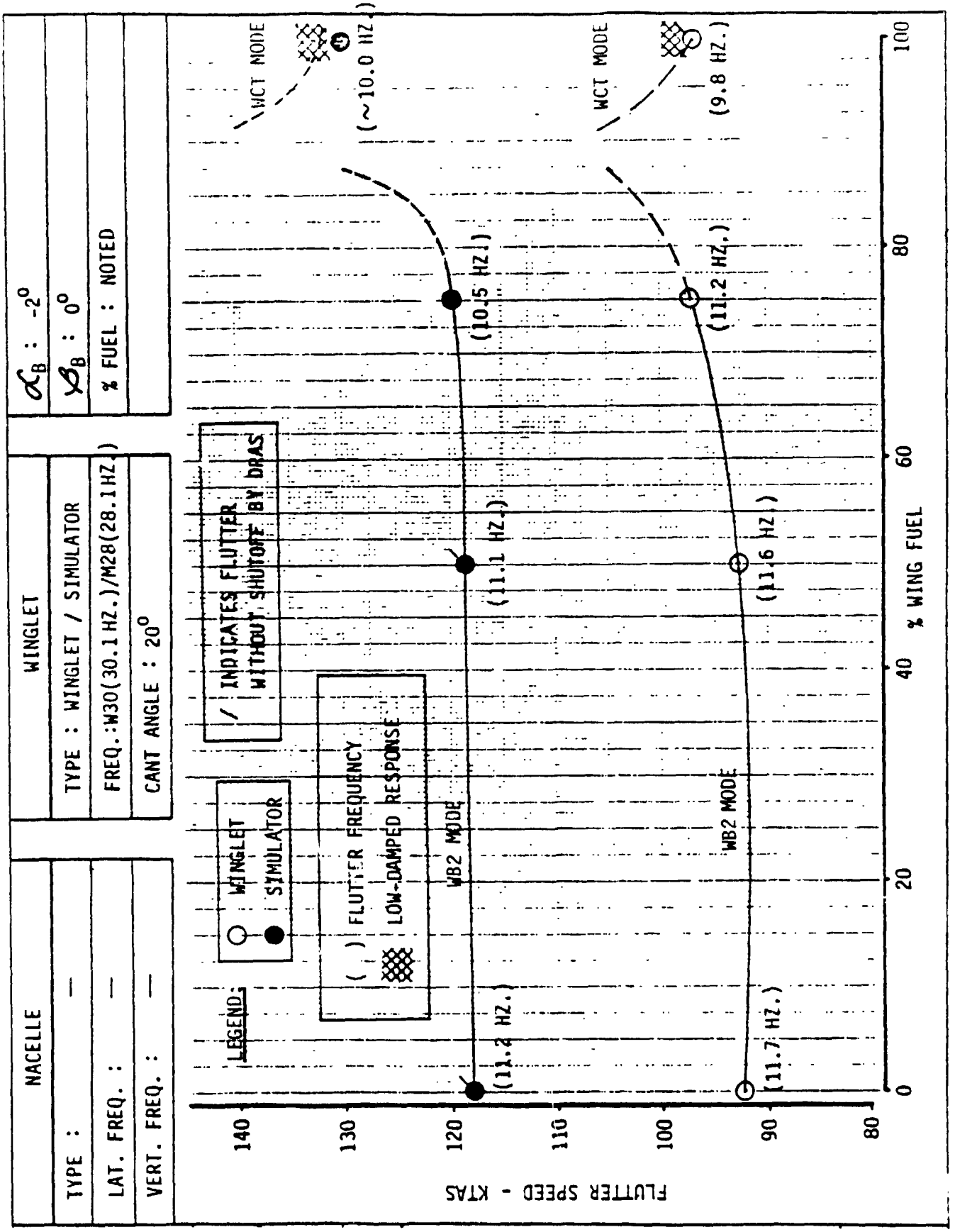

FIGURE 6b TEST FLUTTER SPEEDS VS. PERCENT FUEL, CLEAN WING WITH SIMULATOR/WINGLET (NOMINAL)

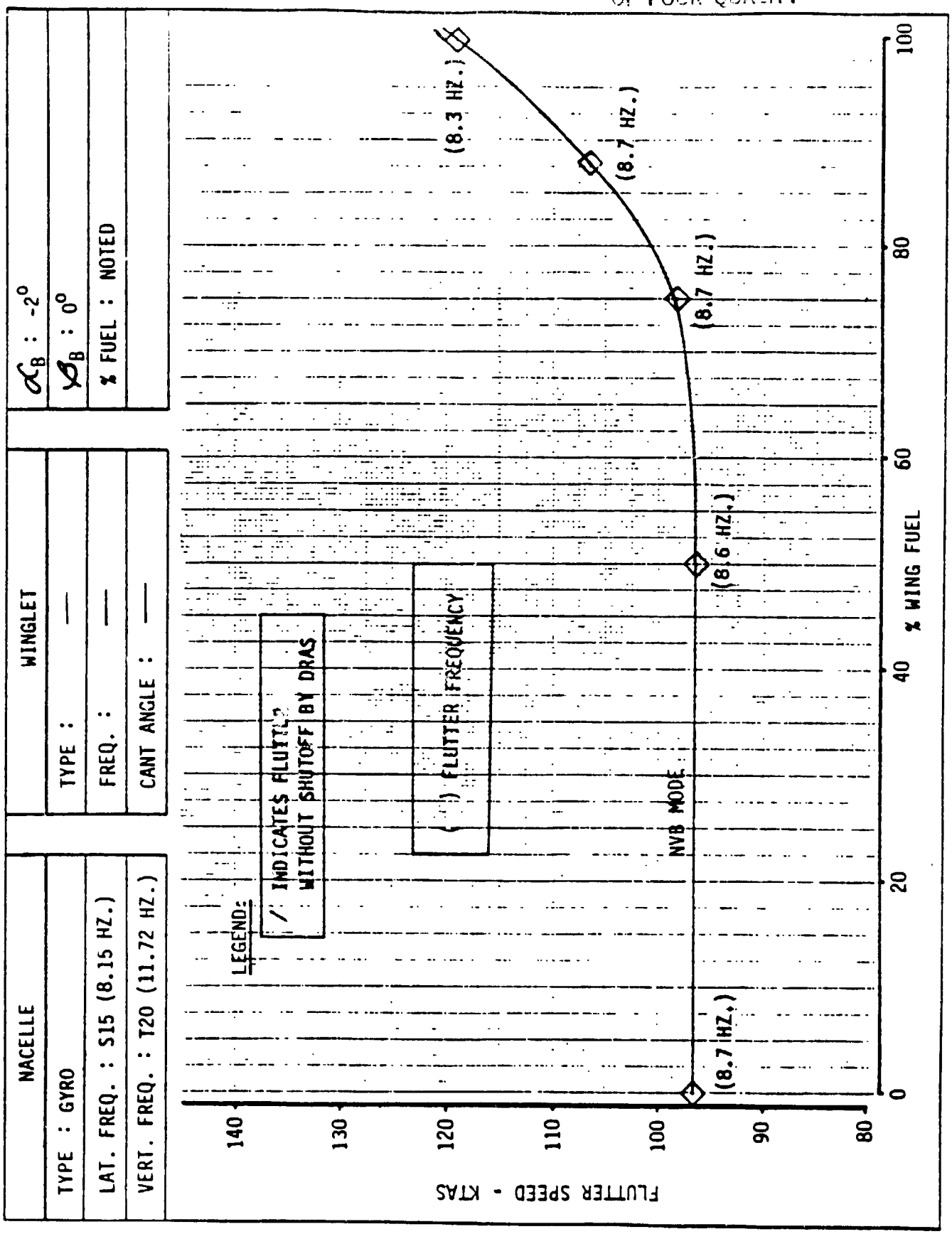

FIGURE 6c TEST FLUTTER SPEEDS VS. PERCENT FUEL, WING-NACELLE (NOMINAL)

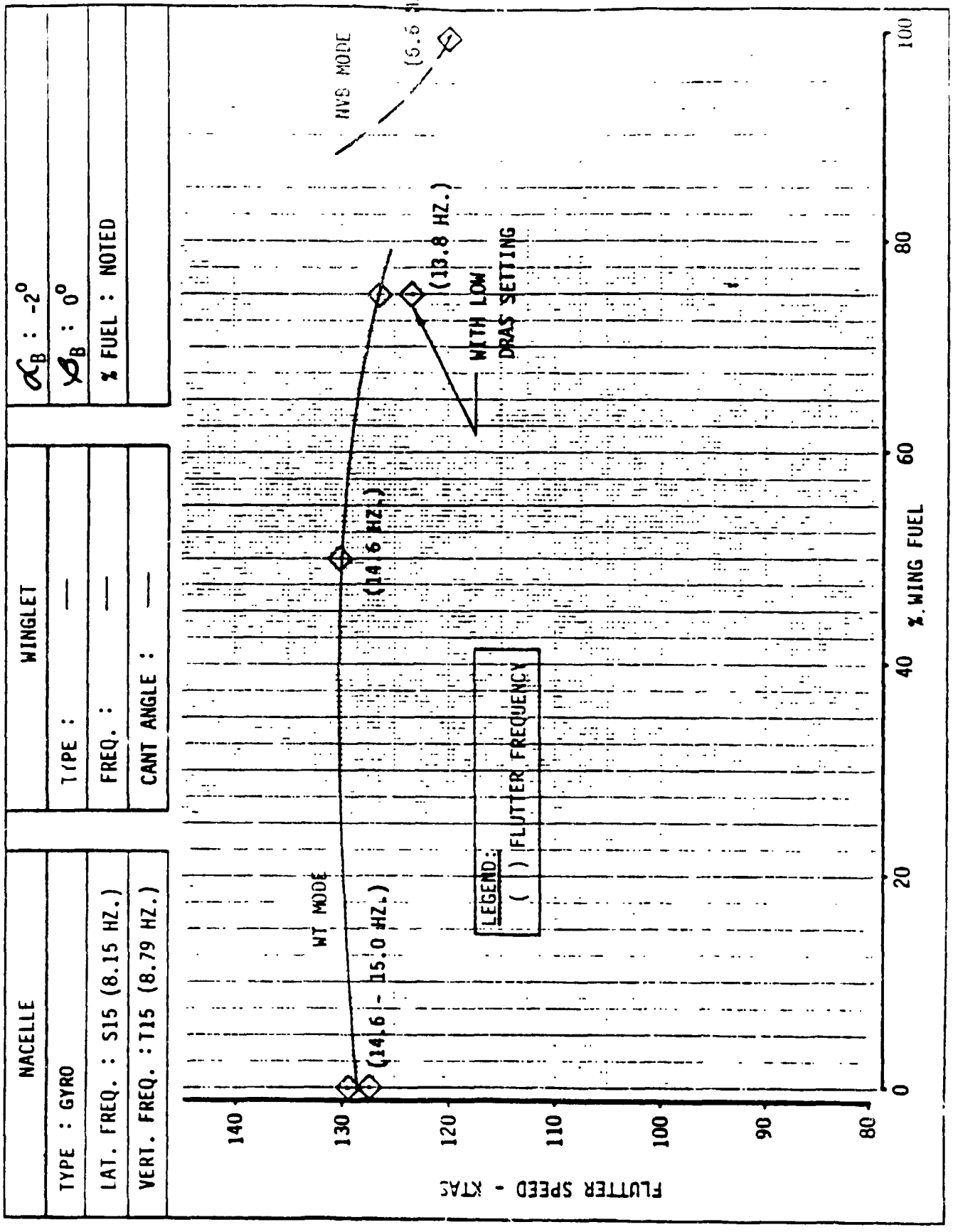

FIGURE 6d TEST FLUTTER SPEEDS VS. PERCENT FUEL, WING-NACELLE (SOFT)

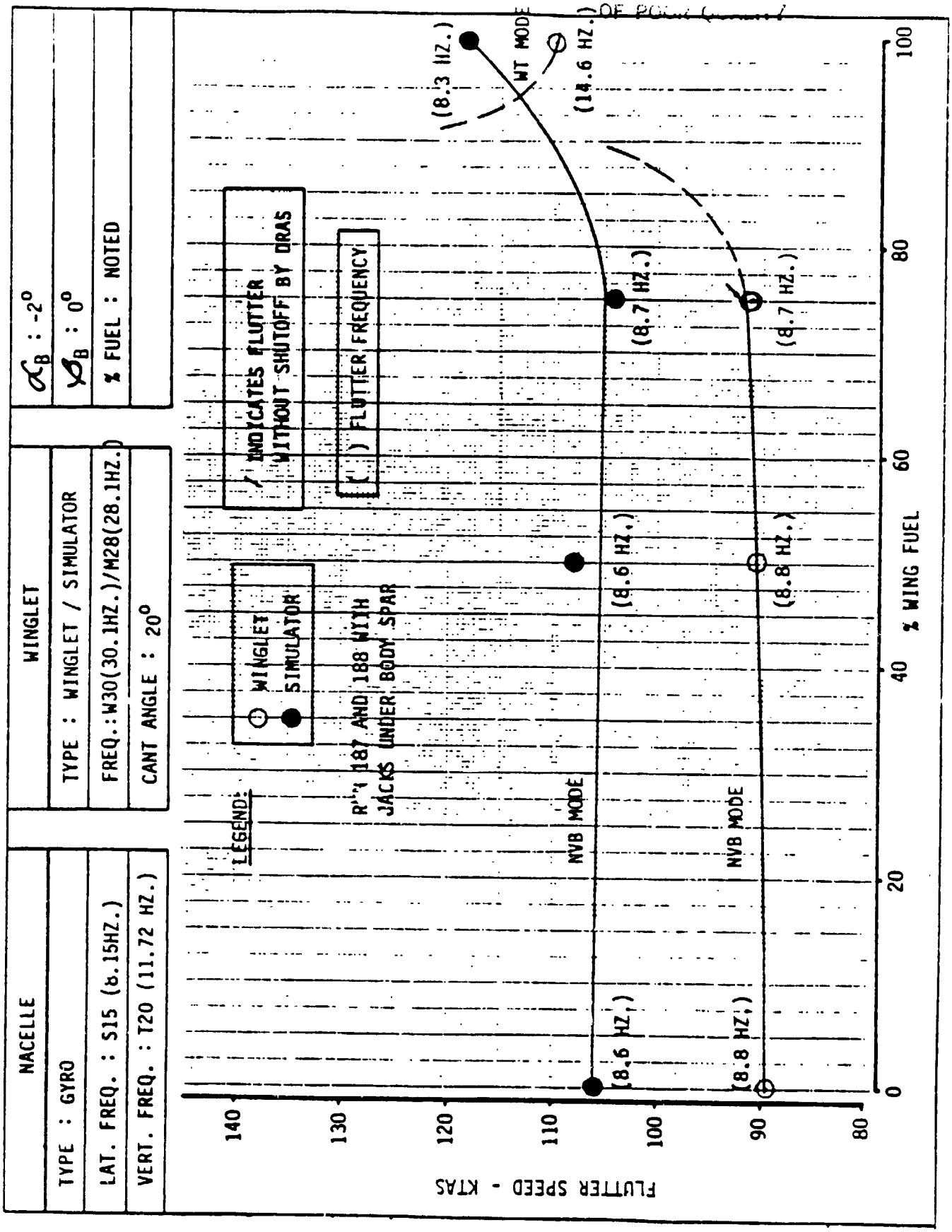

FIGURE 6e TEST FLUTTER SPEEDS VS. PERCENT FUEL, WING-NACELLE (NOMINAL)-SIMULATOR/WINGLET (NOMINAL)

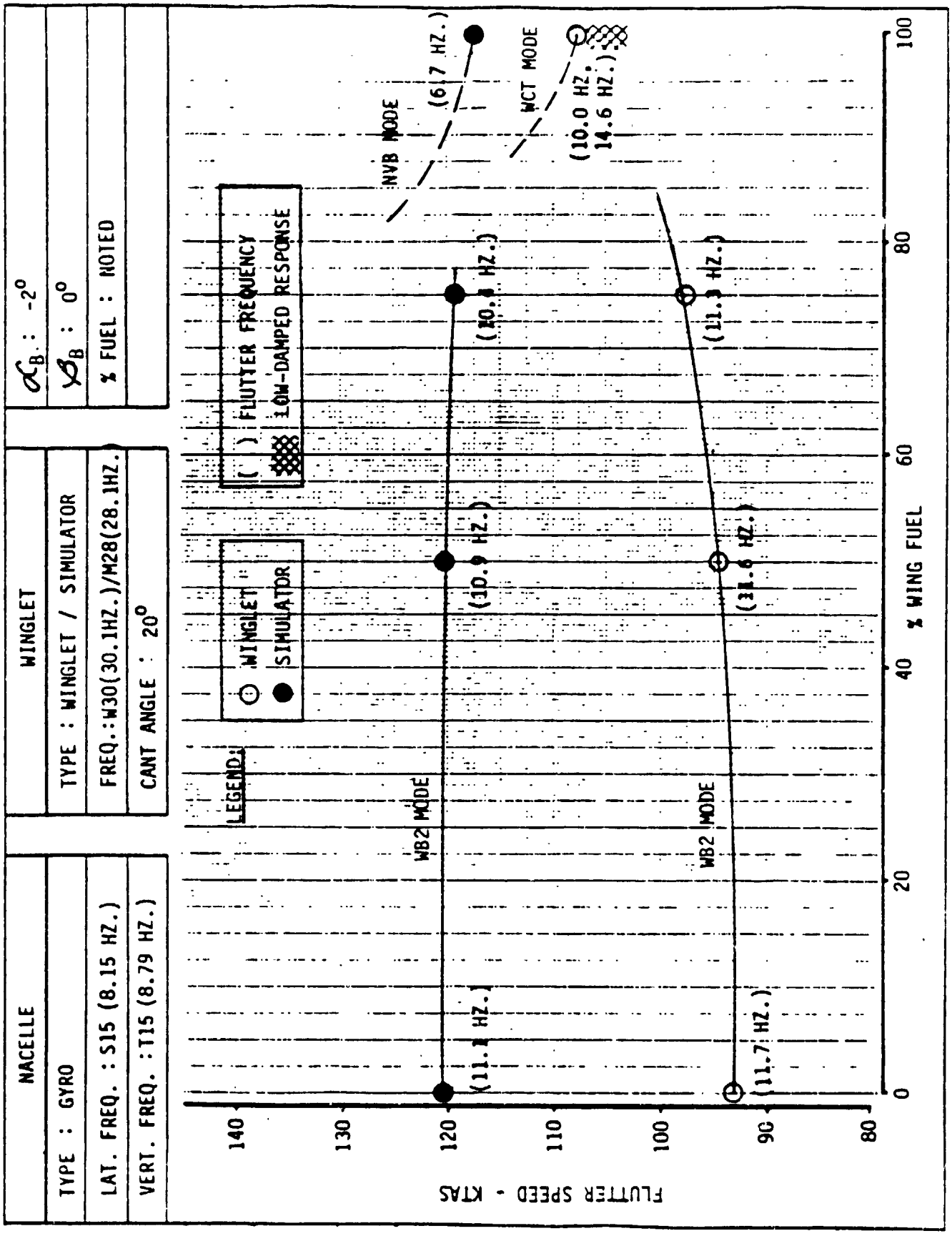

FIGURE 6f TEST FLUTTER SPEEDS VS. PERCENT FUEL, WING-NACELLE SIMULATOR/WINGLET (NOMINAL) (SOFT) -

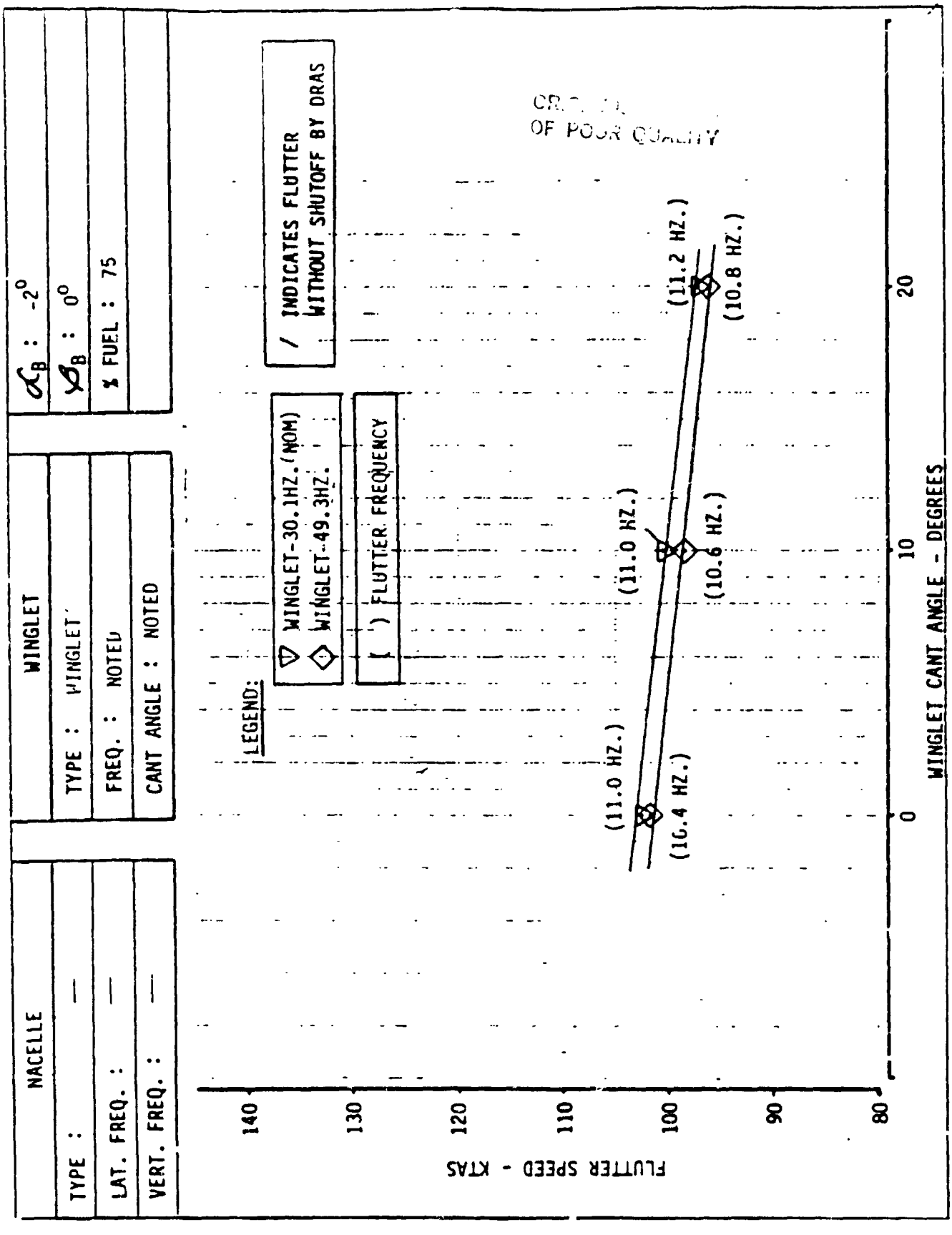

FIGURE 7a CANT ANCLE EFFECT ON FLUTTER, WINC (75% FUEL) - WINGLET

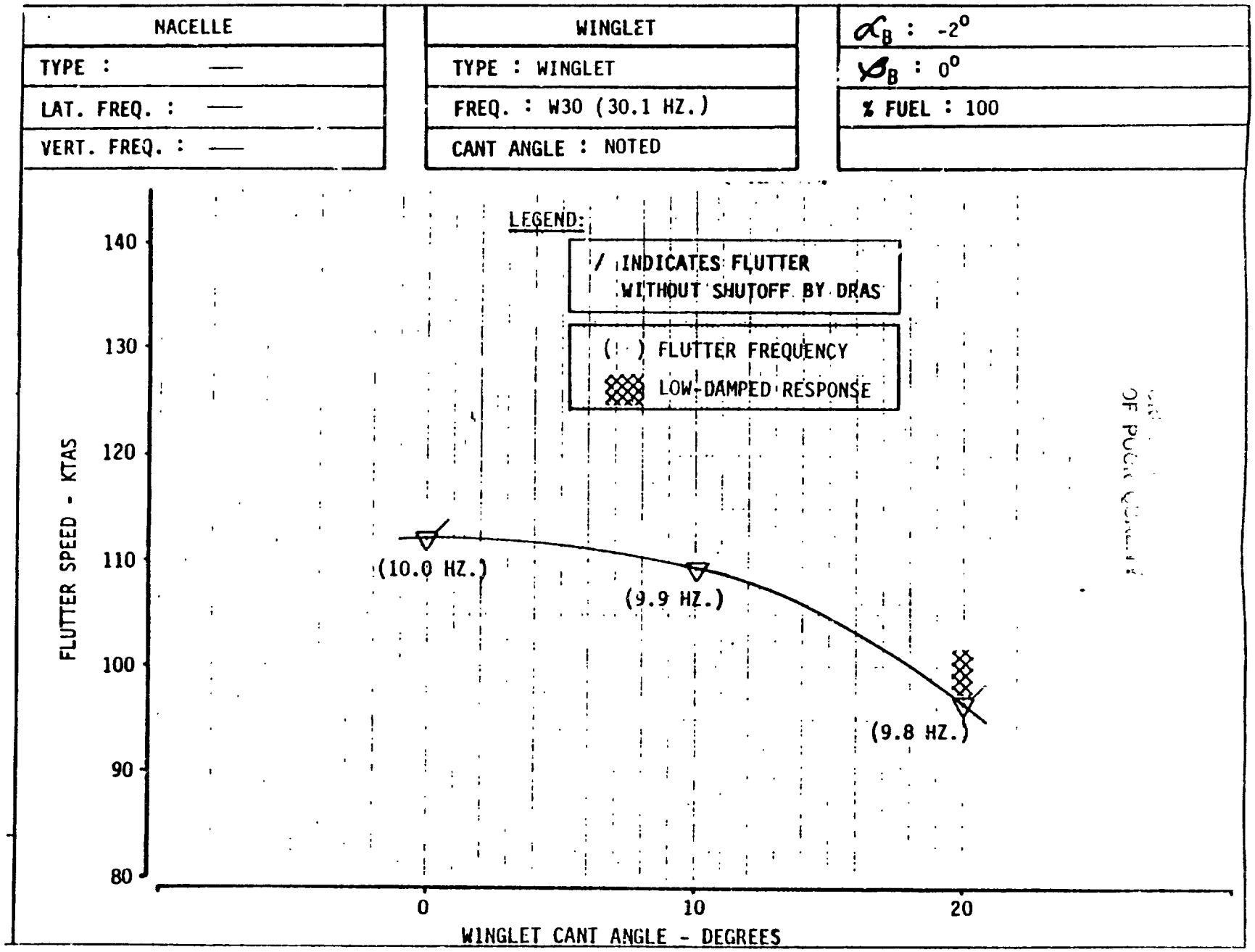

FIGURE 7b CANT ANGLE EFFECT ON FLUTTER, WINC (100% FUEL) - WINGLET

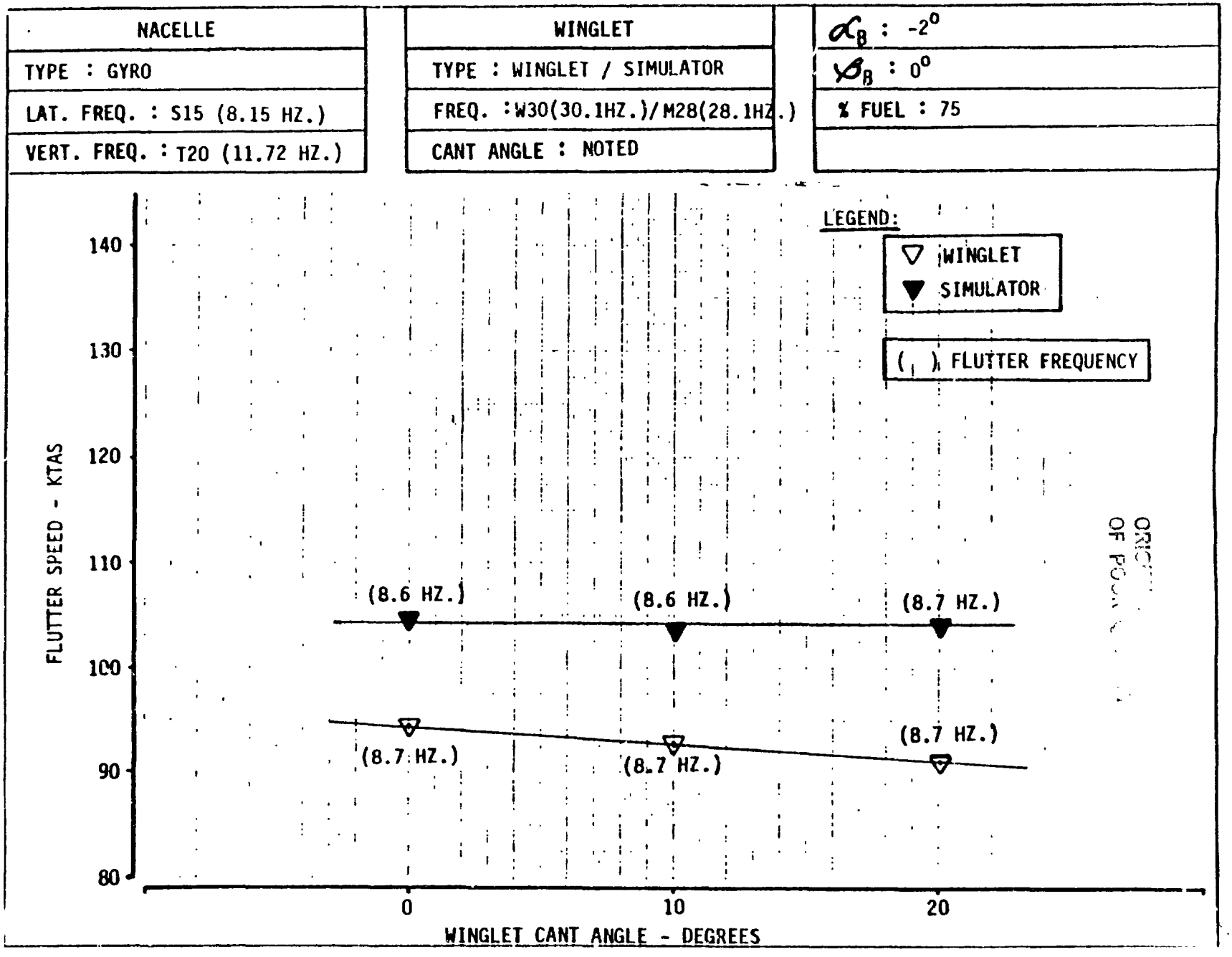

FIGURE 7c CANT ANGLE EFFECT ON FLUTTER, WING (75% FUEL) - NACELLE (NOMINAL) - SIMULATOR/WINGLET

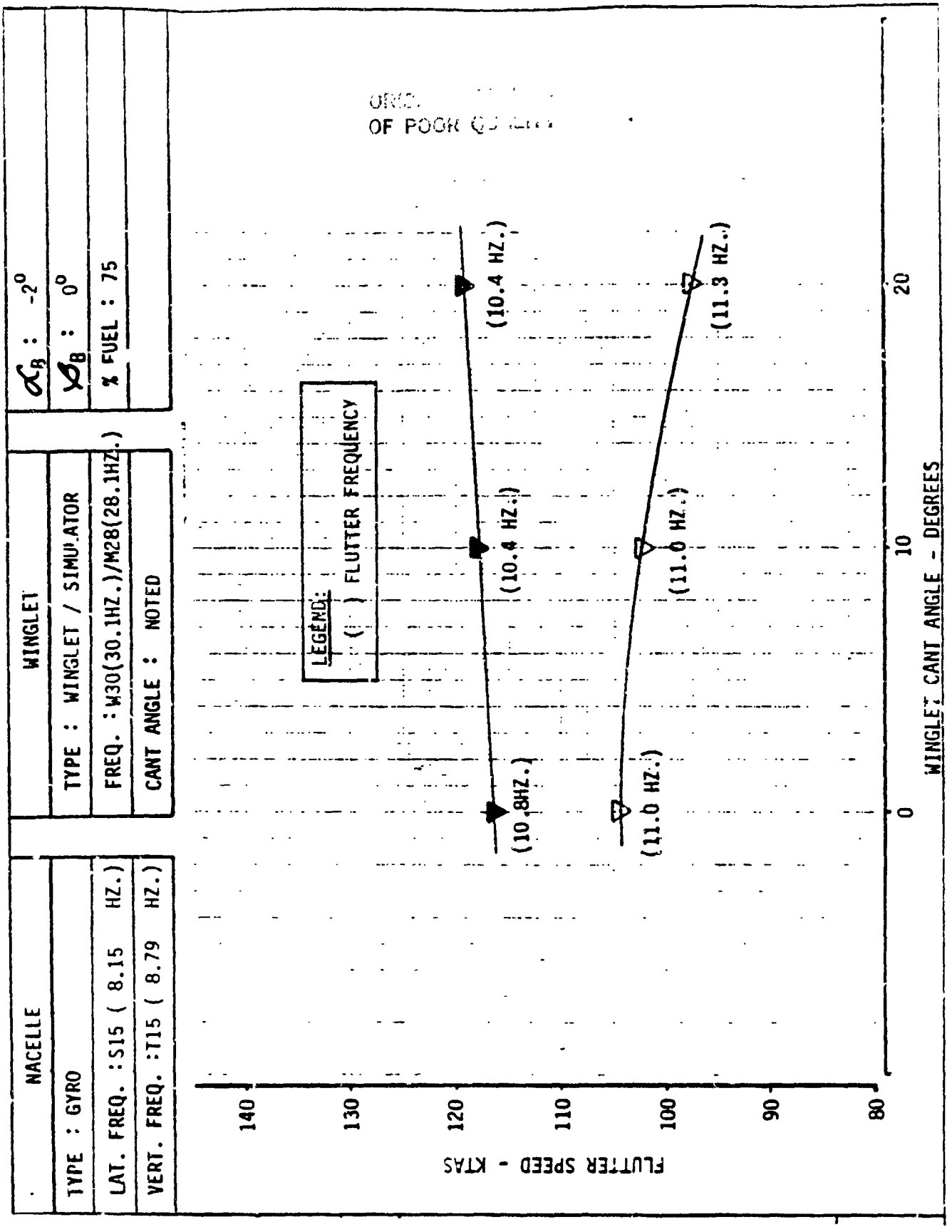

FIGURE 7d CANT ANGLE EFFECT ON FLUTTER, WING (75% FUEL) - NACELLE (SOFT) - SIMULATOR/WINGLET

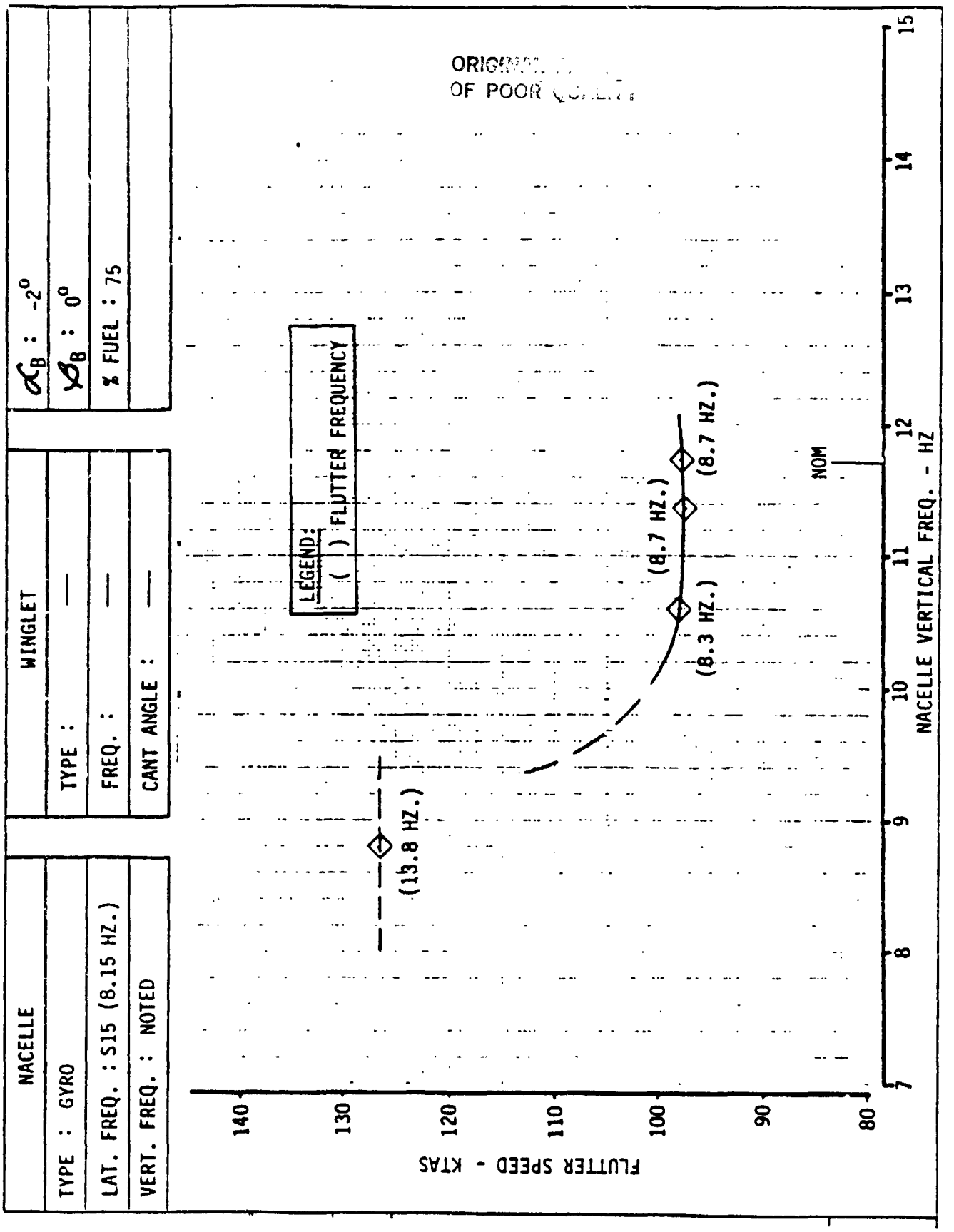

FIGURE 8a WING (75% FUEL) WITH NACELLE, NACELLE VERTICAL BENDING FREQ. VARIATION

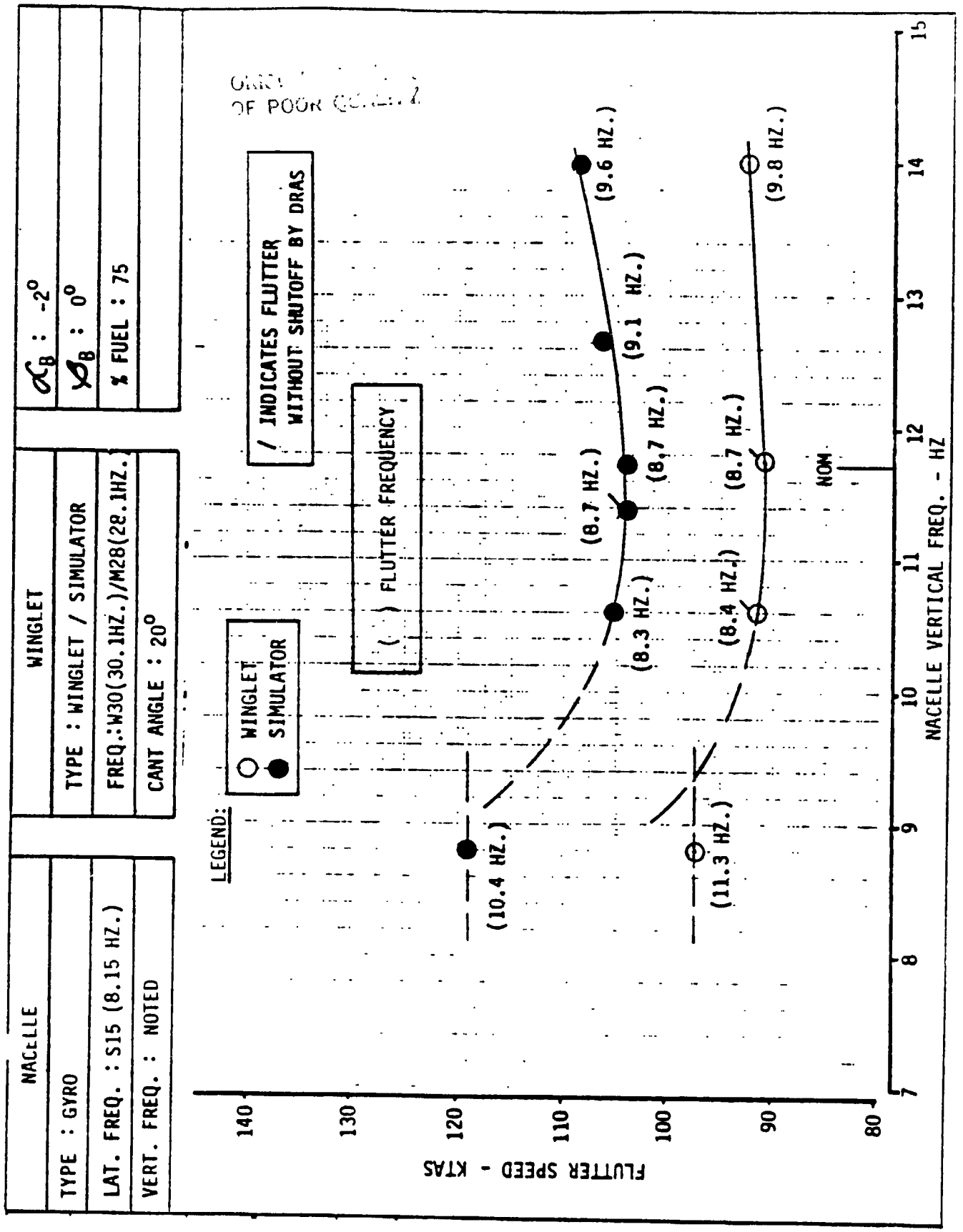

FIGURE 8b WING (75% FUEL) WITH NACELLE AND WINGLET/SIMULATOR, NACELLE VERTICAL BENDING FREQ. VARIATION

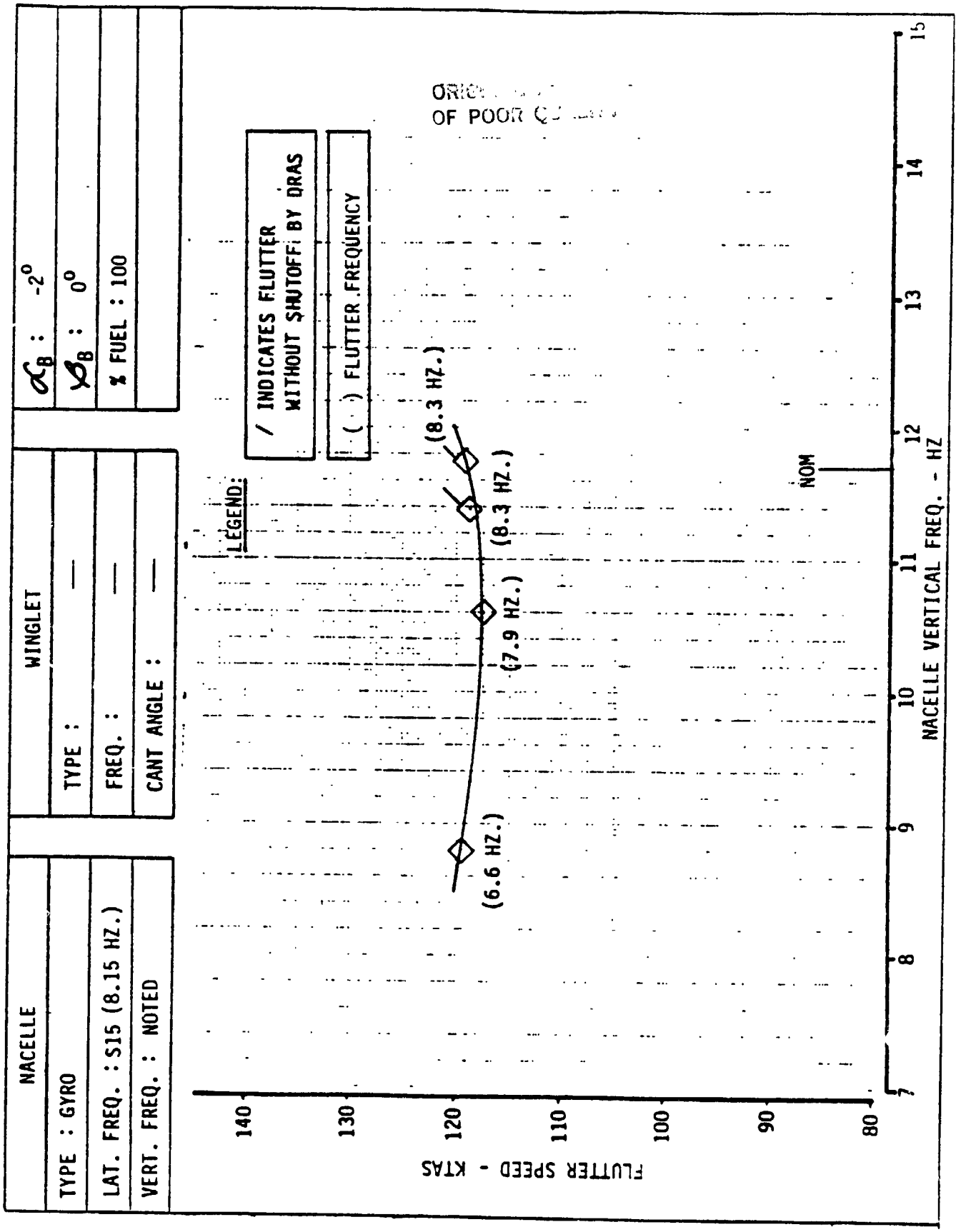

FIGURE 8c WINC (100% FUEL) WITH NACELLE & WINGLET/SIMULATOR, NACELLE VERTICAL BENDING FREQ. VARIATION

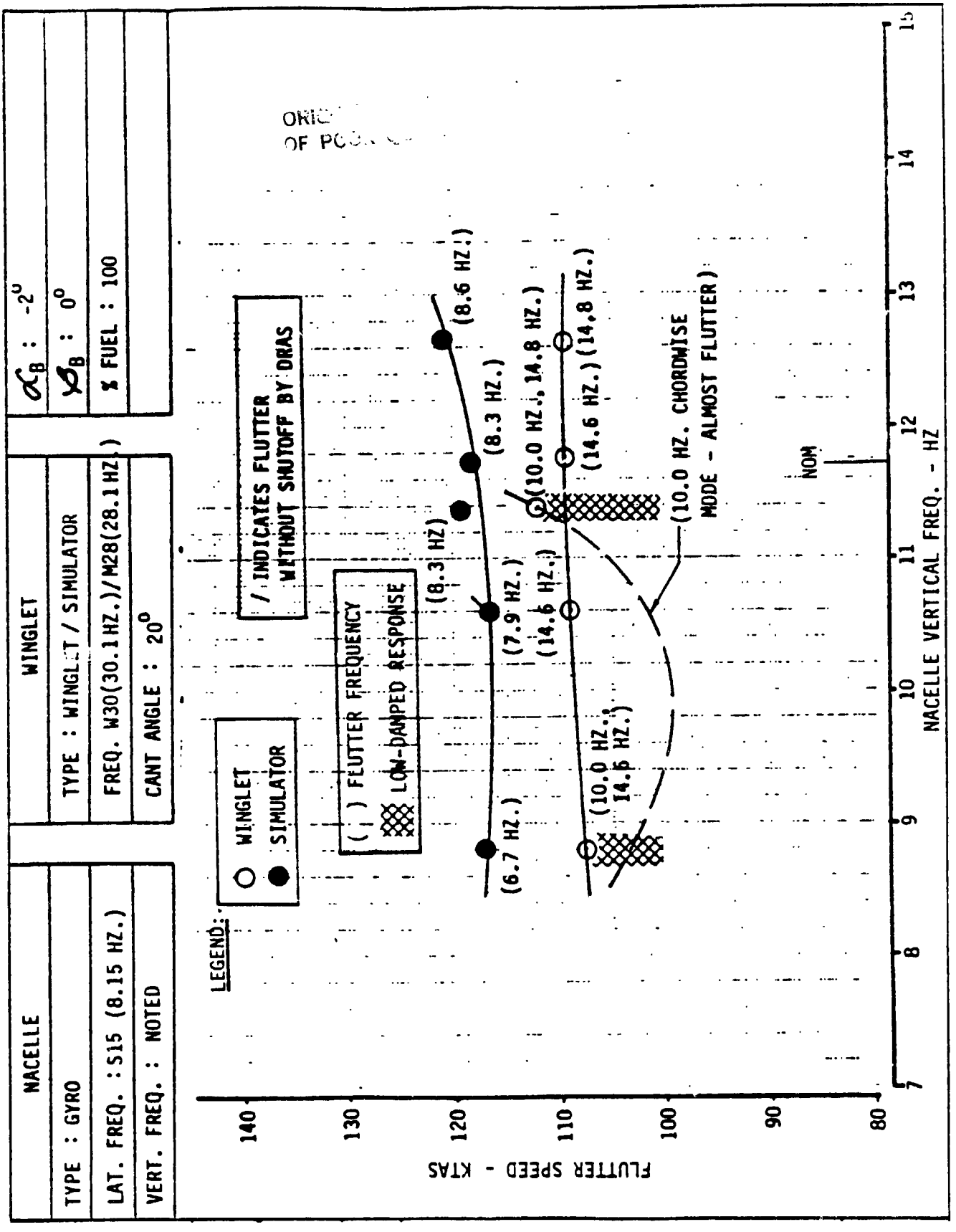

FIGURE 8d WING (100% FUEL) WITH NACELLE & WINGLET/SIMULATOR, NACELLE VERTICAL BENDING FREQUENCY VARIATION

FIGURE 9a WING WITH NACELLE & WINGLET/SIMULATOR, BODY PITCH VARIATION

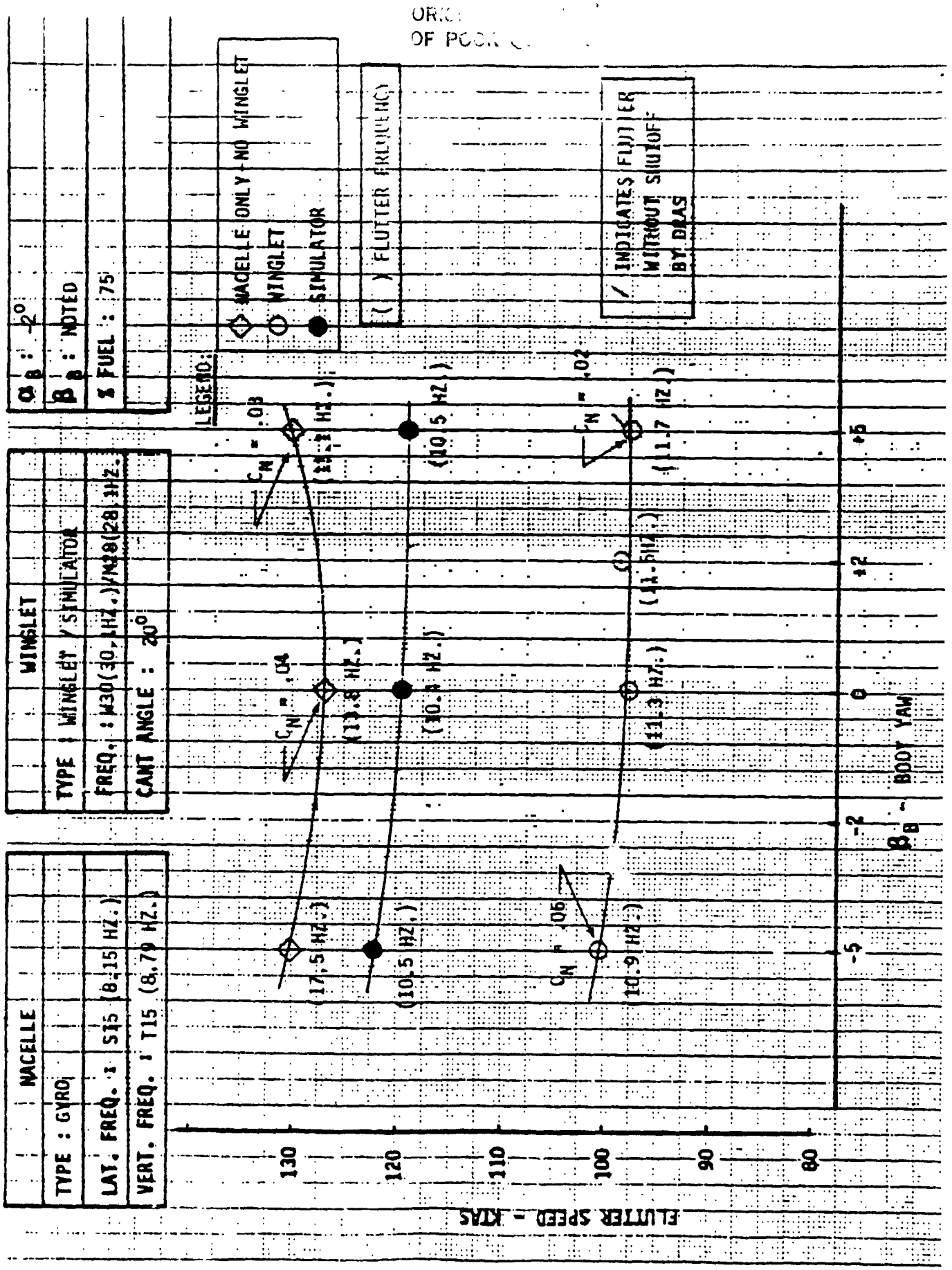

FIGURE 9b WINC WITH NACELLE & WINCLET/SIMULATOR, BODY YAW VARIATION

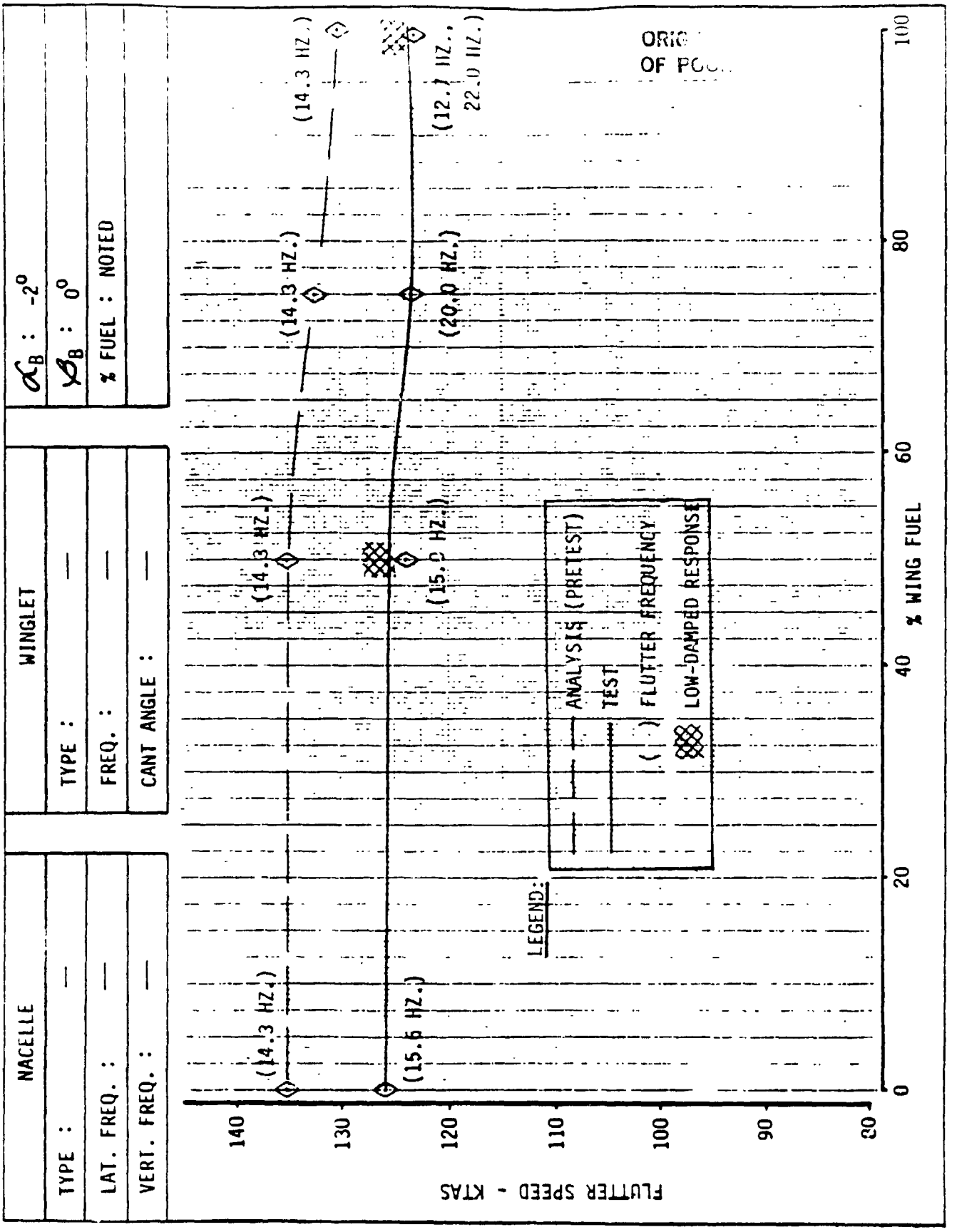

FIGURE 10a ANALYSIS-TEST CORRELATION (PRETEST), CLEAN WING, FUEL VARIATION

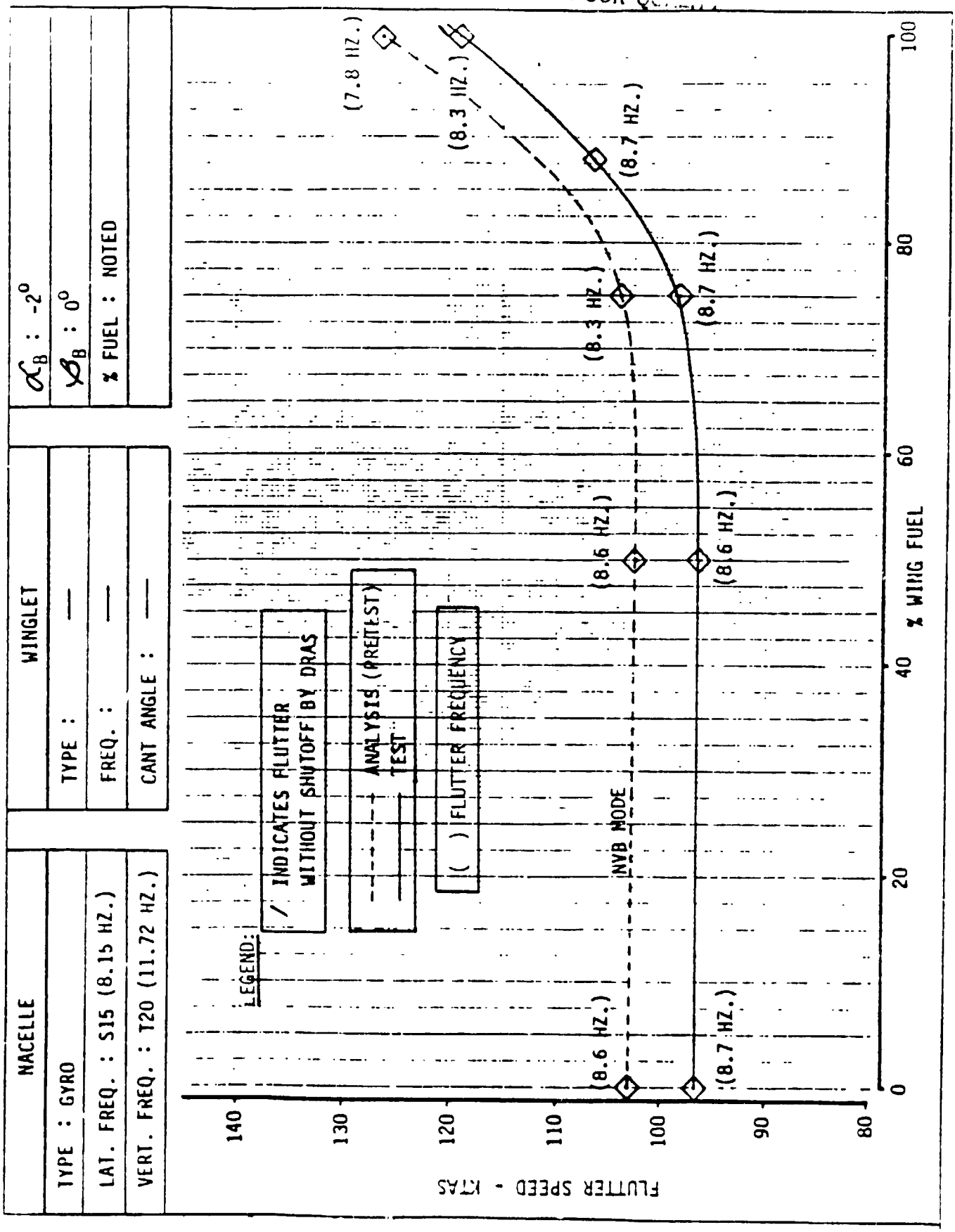

FIGURE 10b ANALYSIS-TEST CORRELATION (PRETEST), WING-NACELLE (NOMINAL), FUEL VARIATION

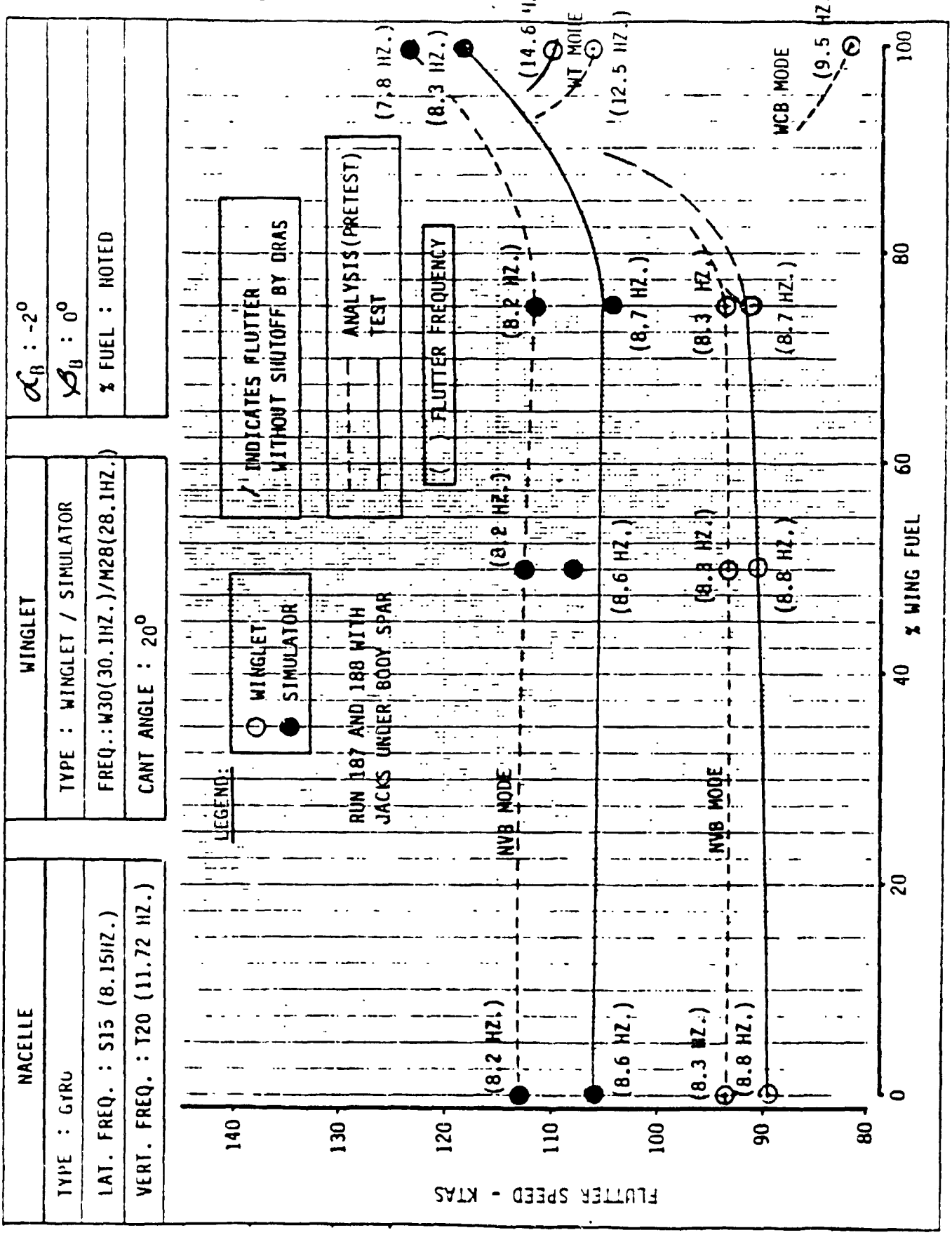

FIGURE 10c ANALYSIS-TEST CORRELATION (PRETEST), WING-NACELLE (NOM) - WINGLET/SIMULATOR (NOM), FUEL VARIATION

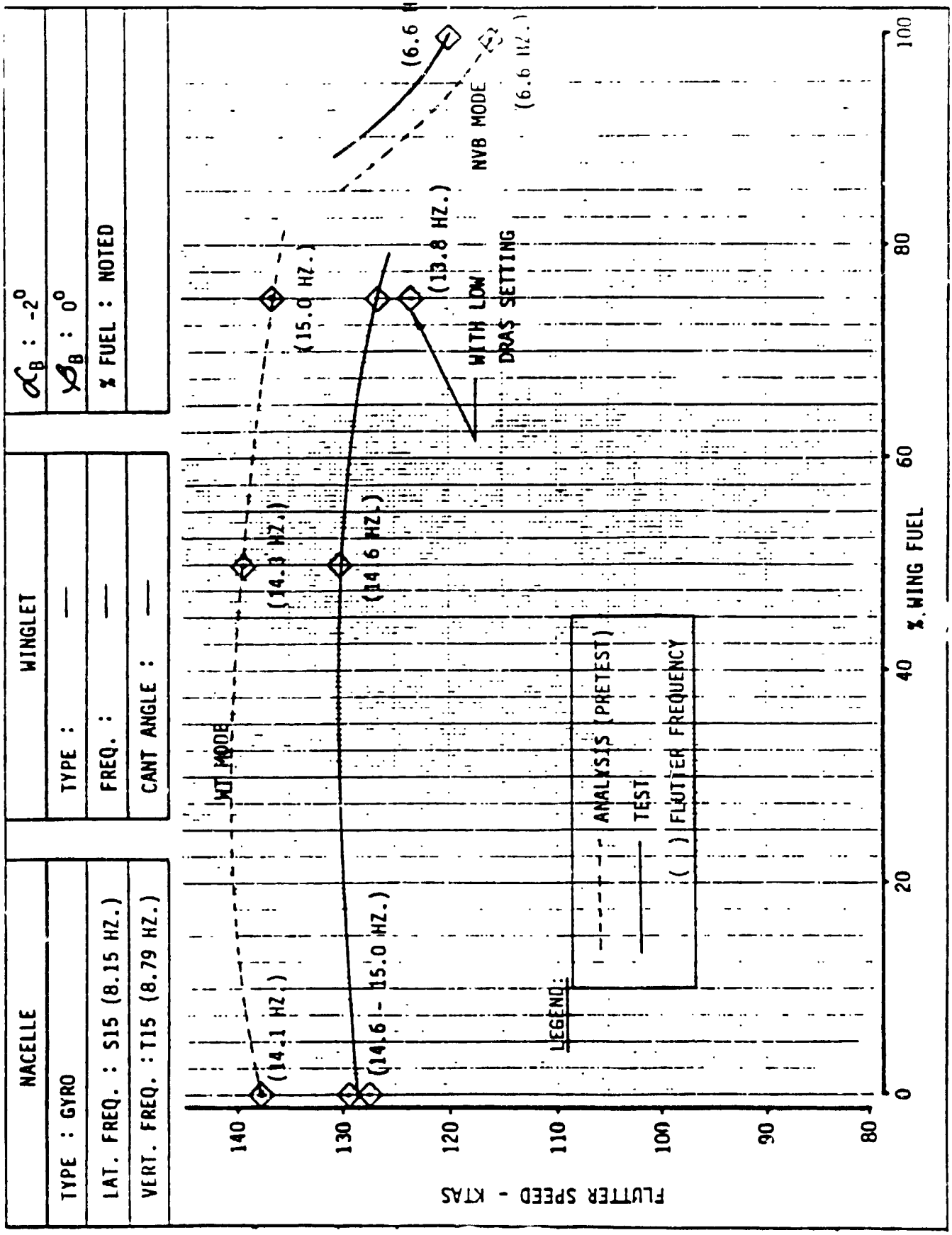

FIGURE 10d ANALYSIS-TEST CORRELATION (PRETEST), WING-NACELLE (SOFT), FUEL VARIATION

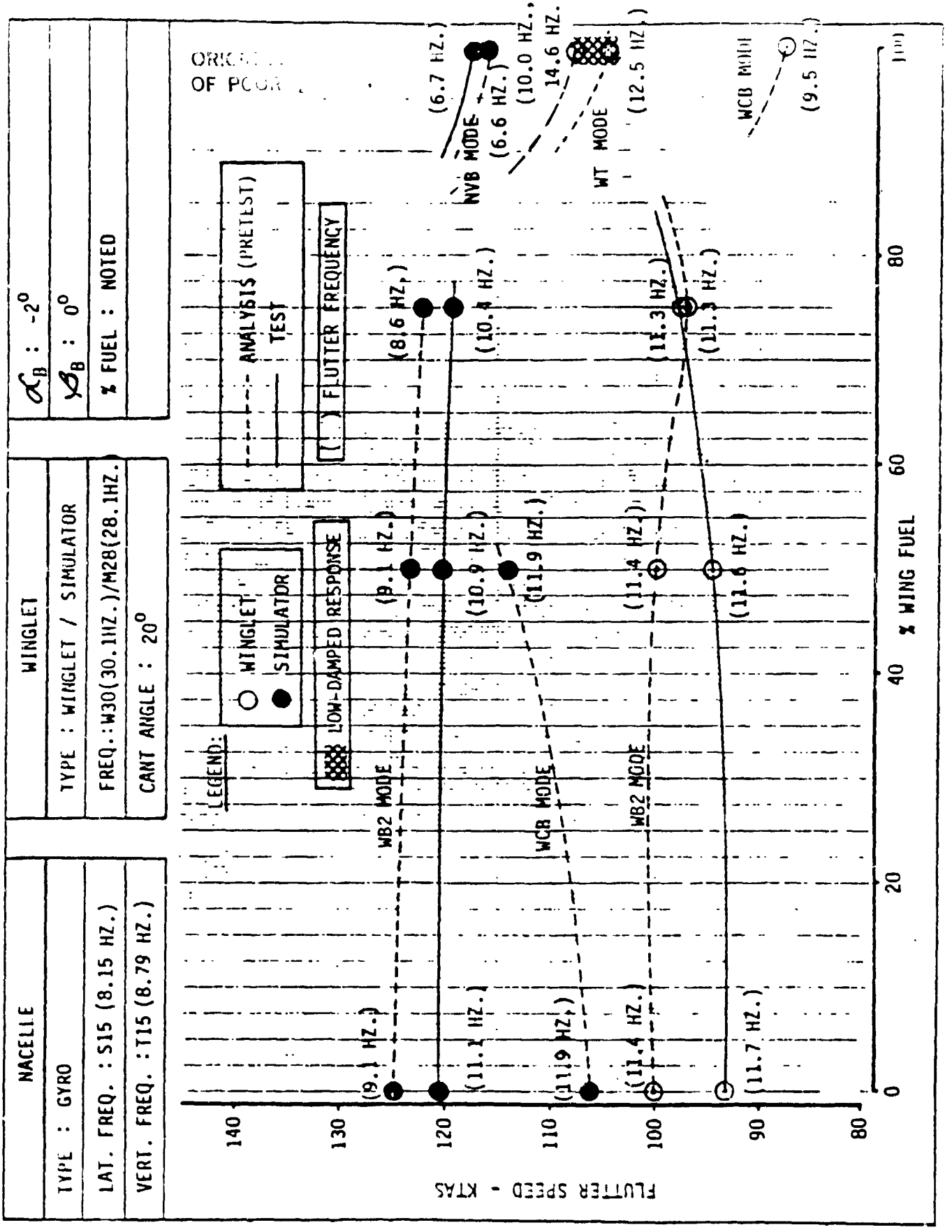

FIGURE 10e ANALYSIS-TEST CORRELATION (PRETEST), WING-NACELLE (SOFT)-WINGLET/SIMULATOR (NOM), FUEL VARIATION

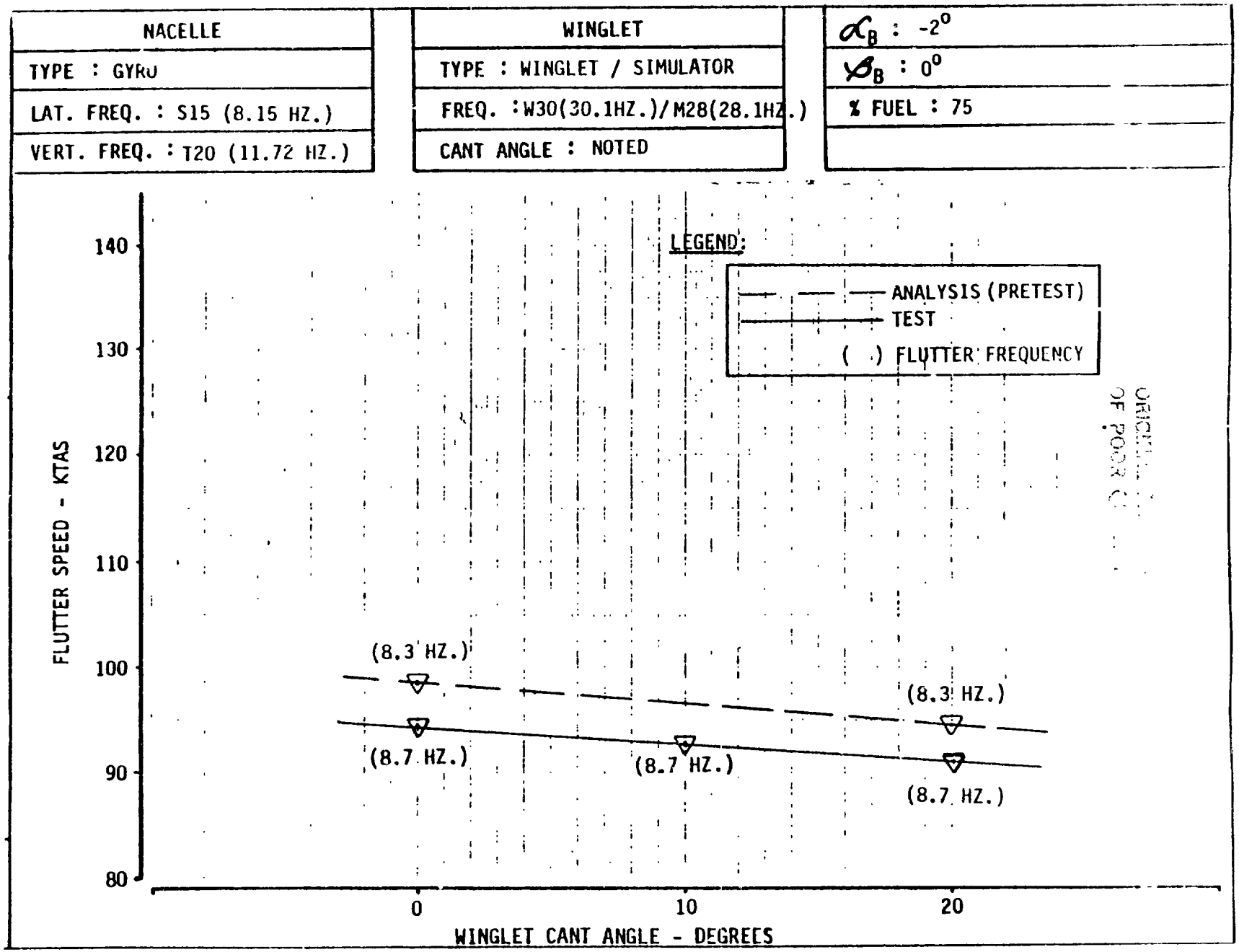

FIGURE 10f WINC (75% FUEL) - NACELLE (NOM) - WINGLET/ SIMULATOR, CANT ANGLE VARIATION

NACELLE	WINGLET	α_B : -2^0
TYPE : GYRO	TYPE : WINGLET / SIMULATOR	β_B : 0^0
LAT. FREQ. :S15 (8.15 HZ.)	FREQ. :W30(30.1HZ.)/M28(28.1HZ.)	% FUEL : 75
VERT. FREQ. :T15 (8.79 HZ.)	CANT ANGLE : NOTED	

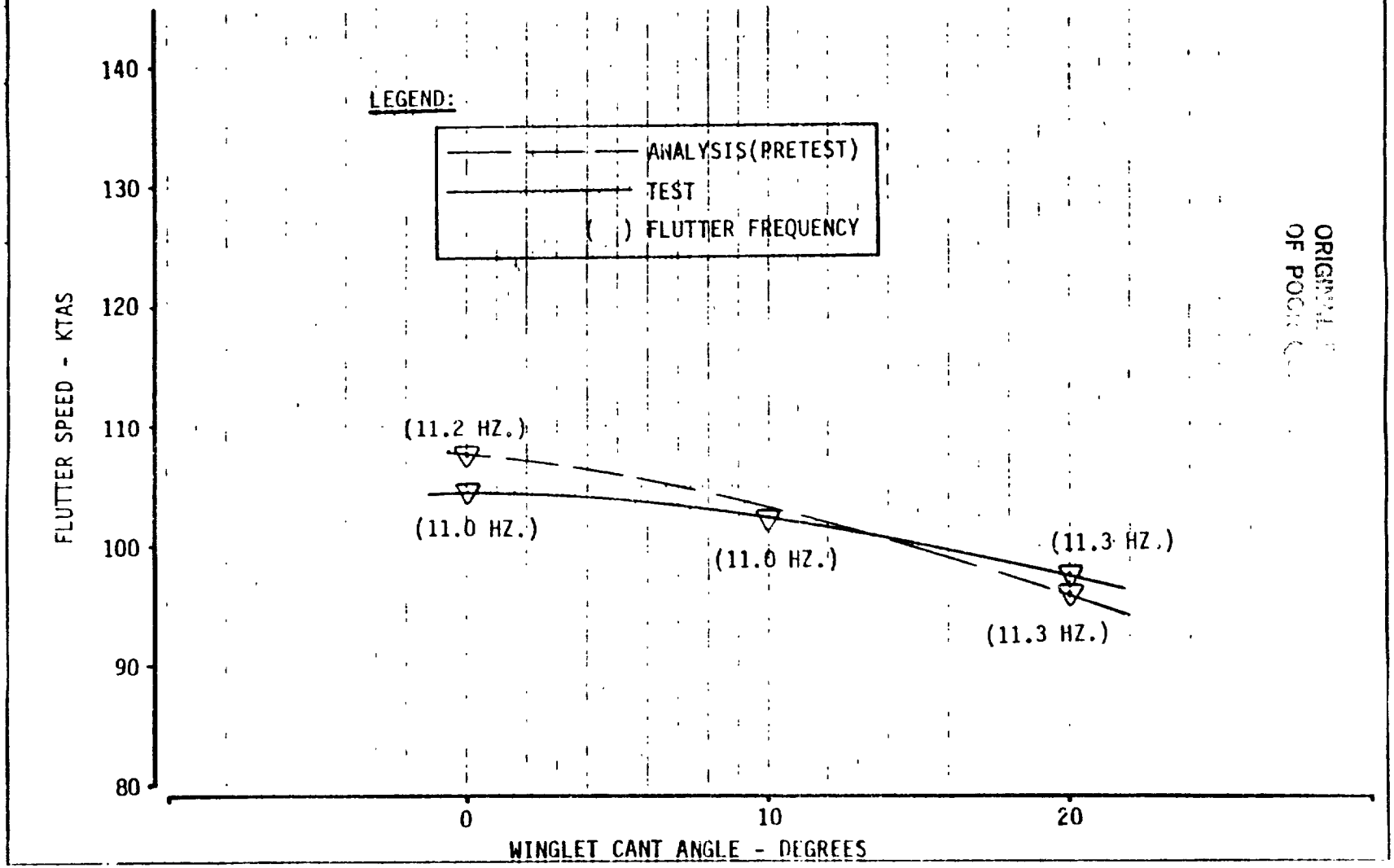

FIGURE 10g KINC (75% FUEL) - NACELLE (SOFT) - WINGLET/ SIMULATOR, CANT ANGLE VARIATION

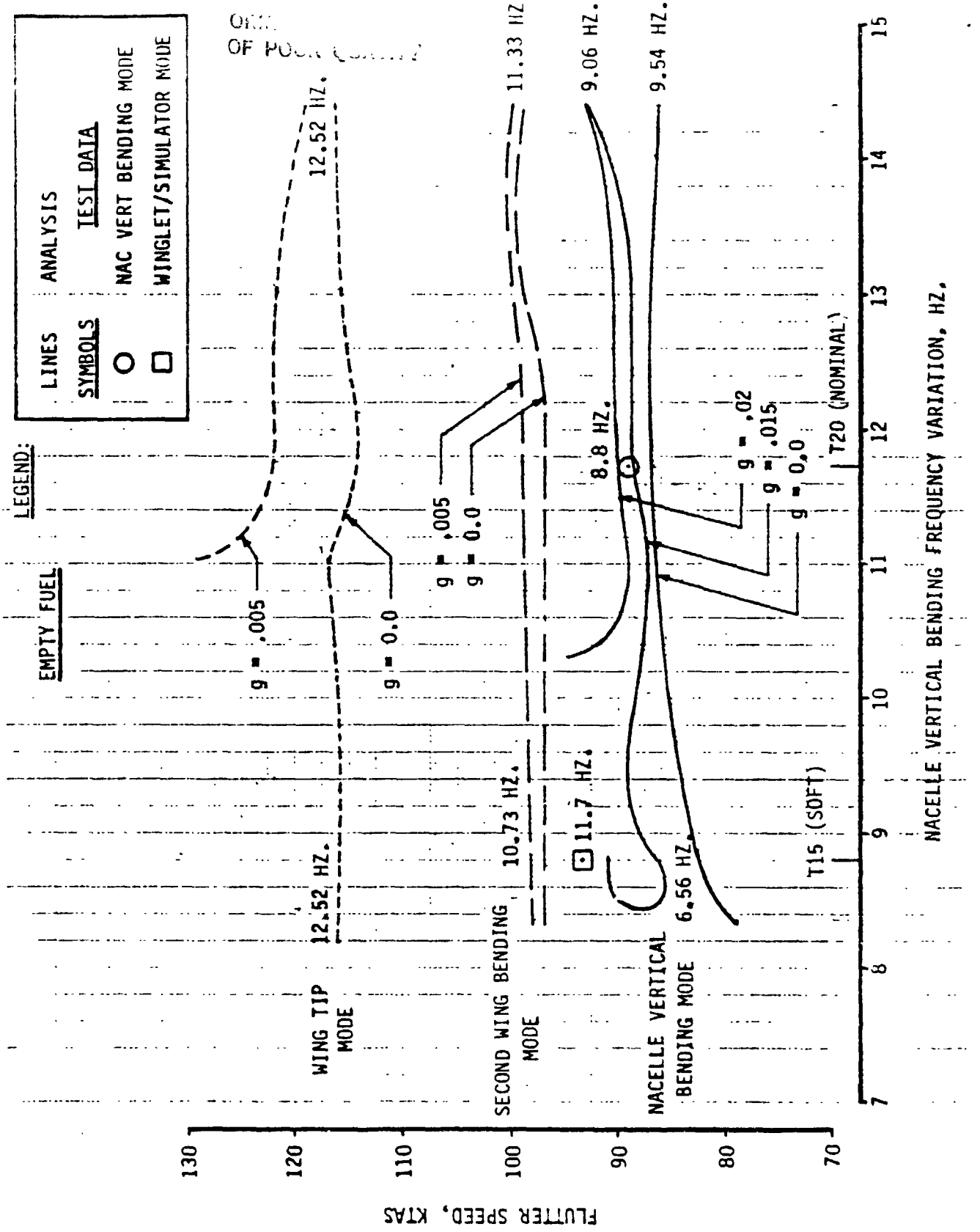

FIGURE 11a ANALYSIS-TEST CORRELATION (POST-TEST), WING (EMPTY)-NACELLE (NOM)-WINGLET (NOM), NACELLE VERTICAL BENDING VARIATION

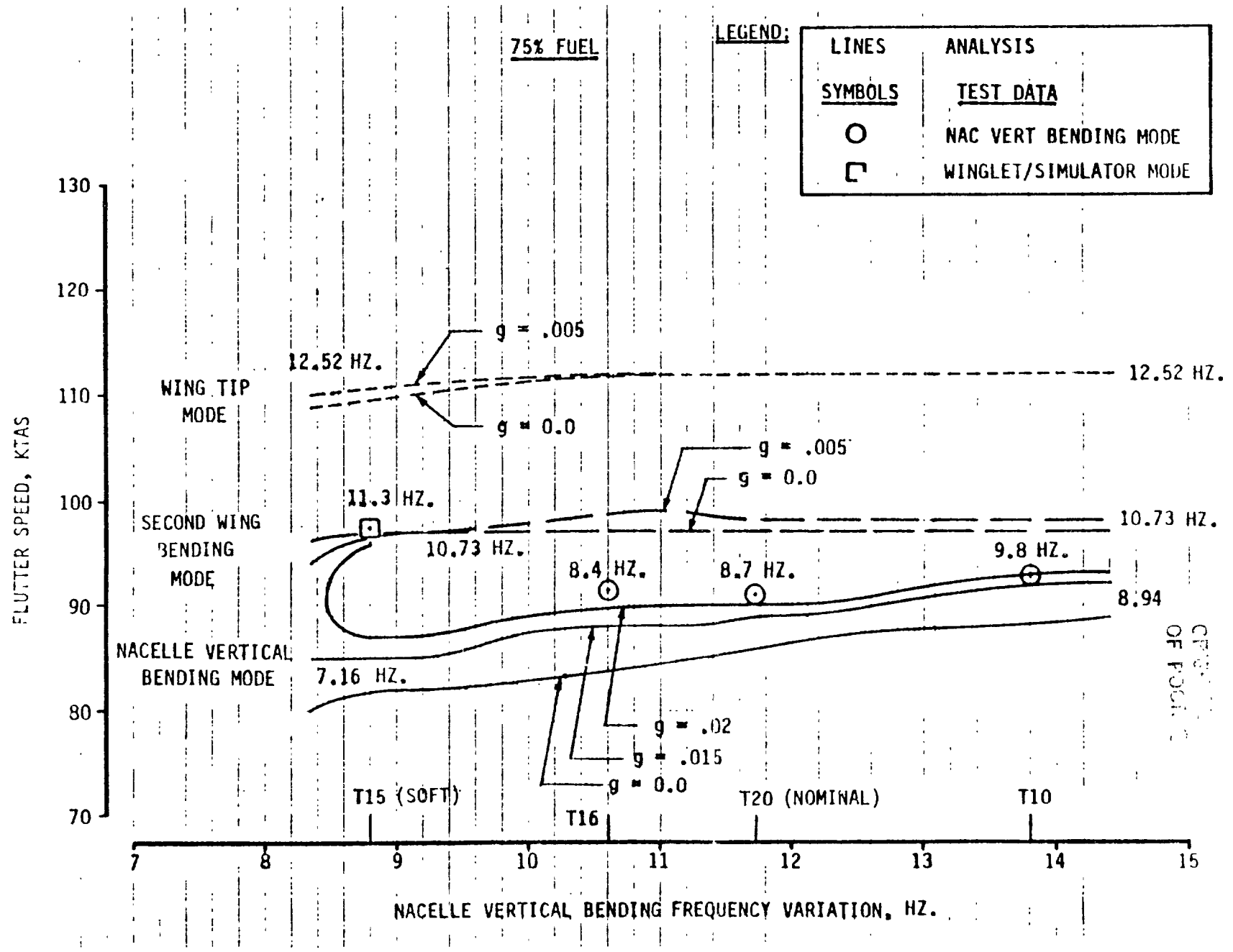

FIGURE 11b ANALYSIS-TEST CORRELATION (POST-TEST), WINC (75% FUEL) - NACELLE (NOM)-WINGLET (NOM), NACELLE VERTICAL BENDING VARIATION

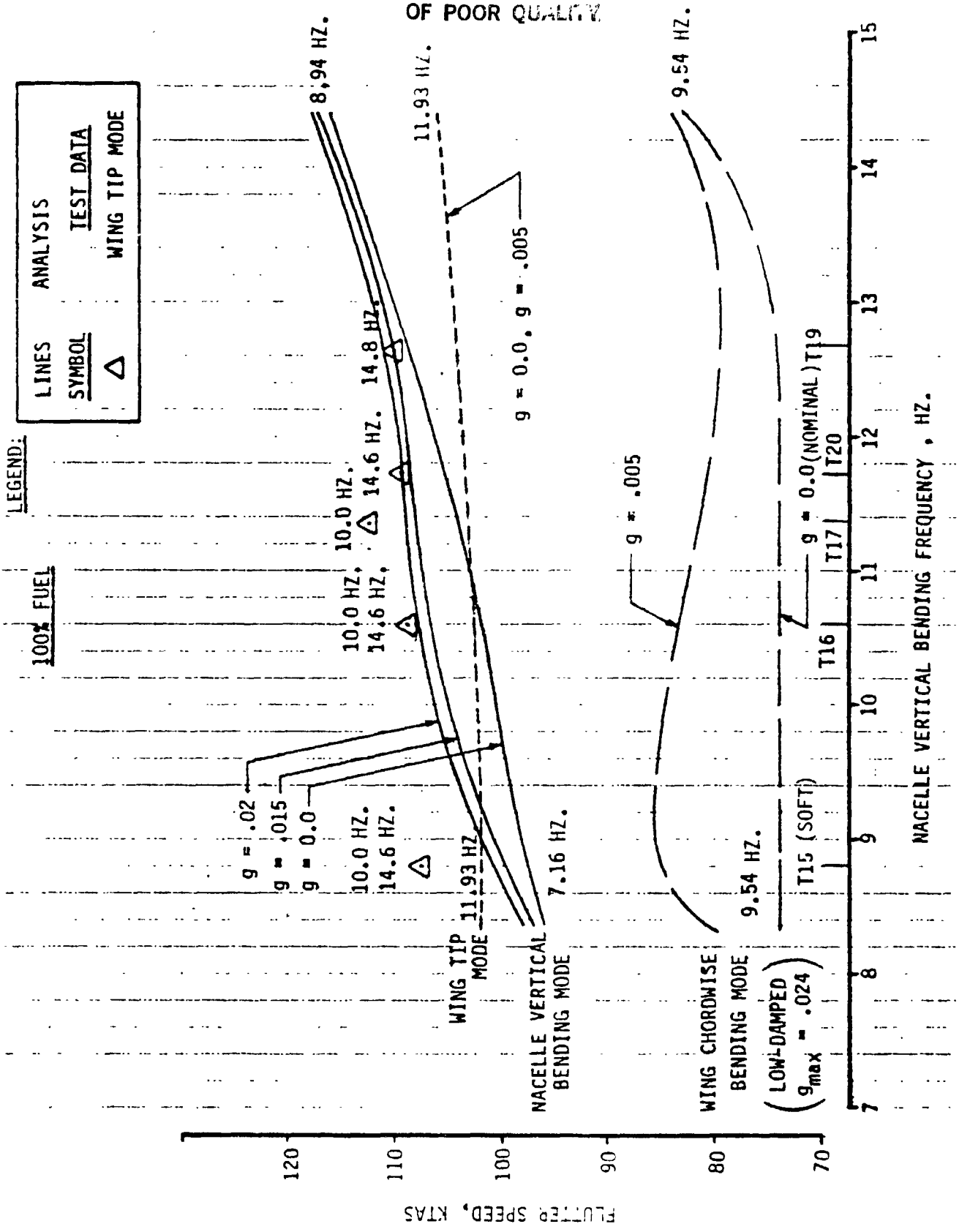

FIGURE 11c ANALYSIS-TEST CORRELATION (POST-TEST), WING (100% FUEL)-NACELLE (NOM)-WINGLET (NOM), NACELLE VERTICAL BENDING VARIATION

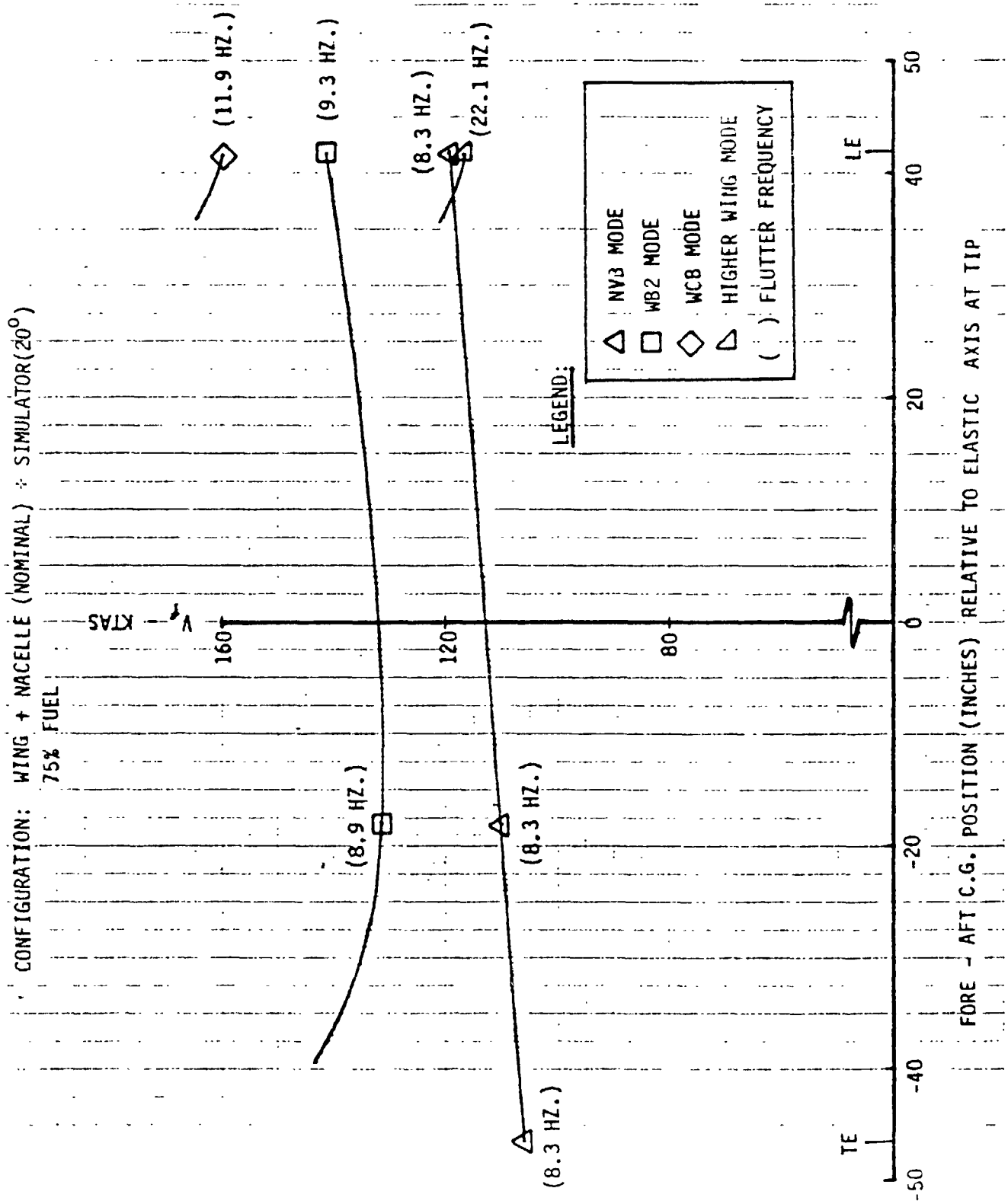

FIGURE 12a ANALYTICAL FLUTTER SENSITIVITY TO FORE-AFT CG LOCATION OF SIMULATOR WEIGHT

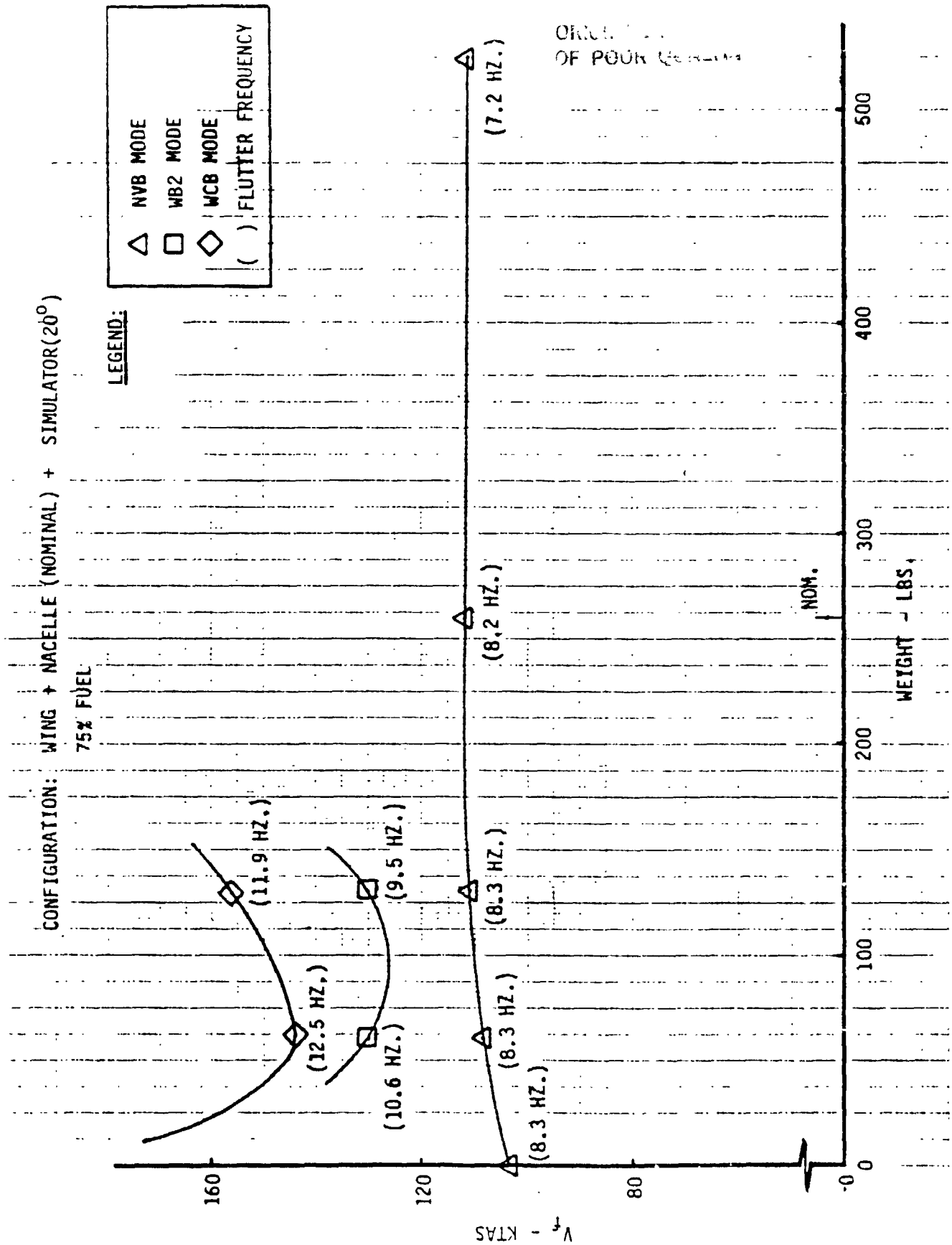

FIGURE 12b ANALYTICAL FLUTTER SENSITIVITY TO SIMULATOR WEICHT

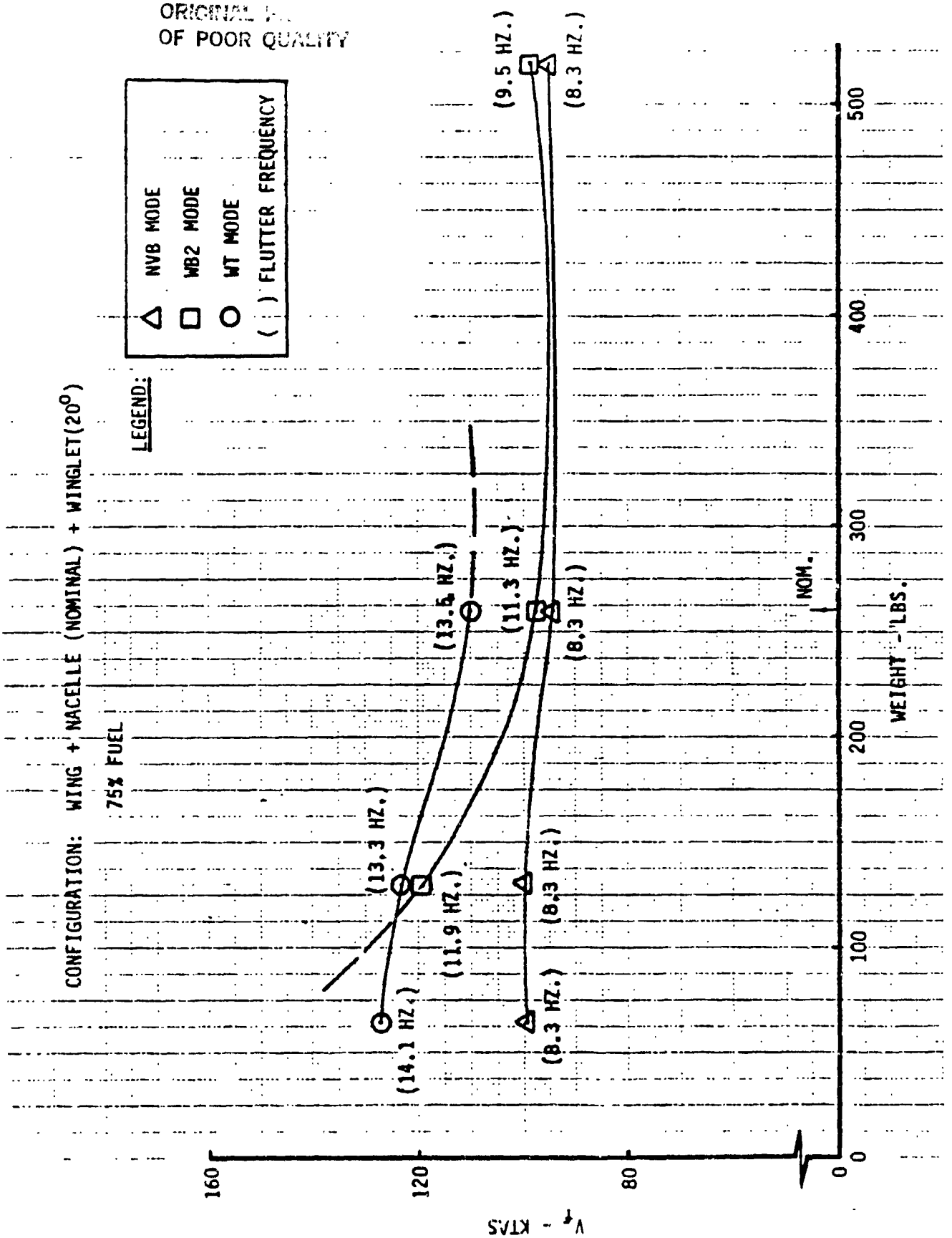

FIGURE 12c ANALYTICAL FLUTTER SENSITIVITY TO WINGLET WEIGHT

APPENDIX

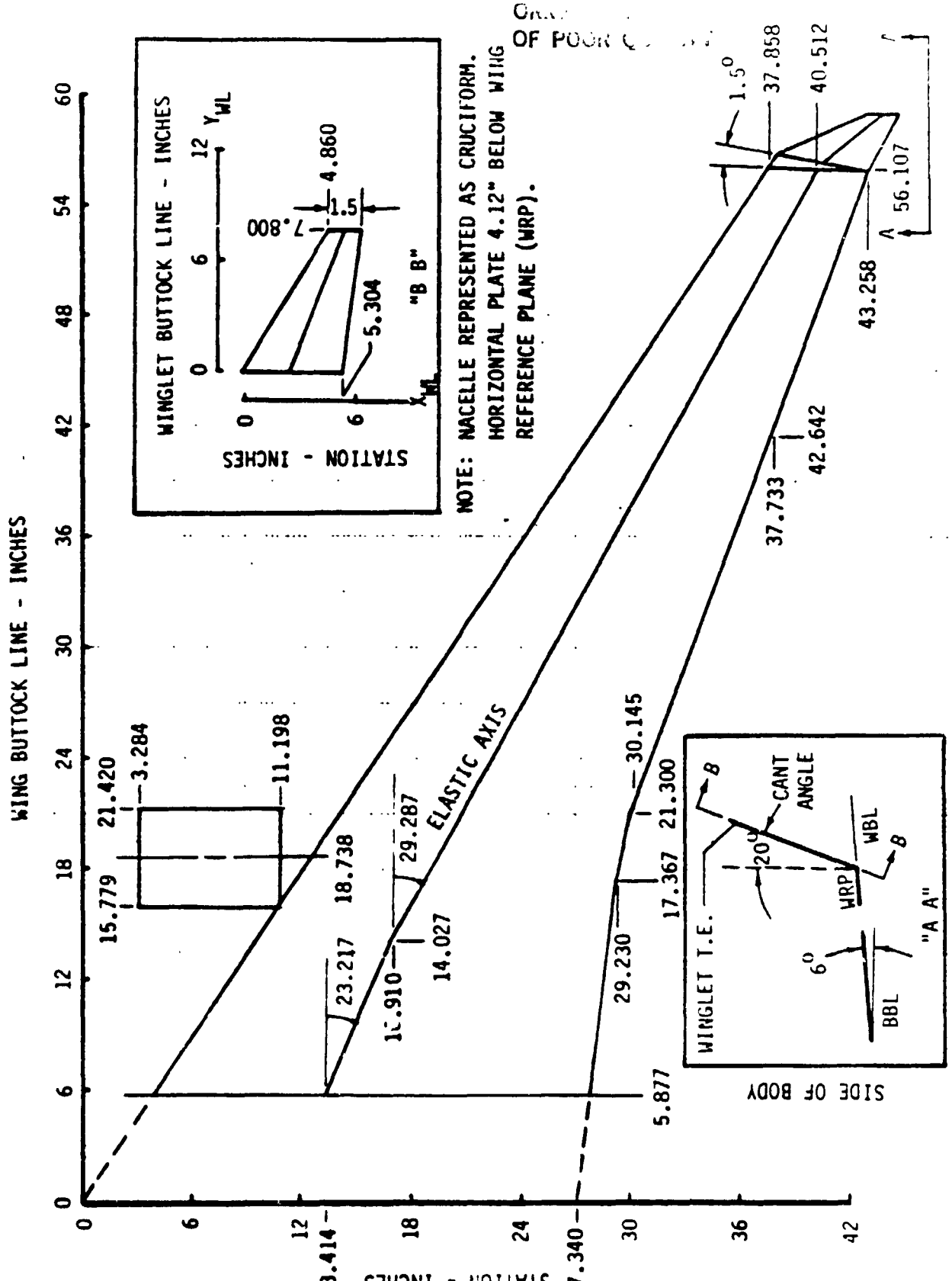

FIGURE A1 GEOMETRY OF WING, WINGLET AND NACELLE

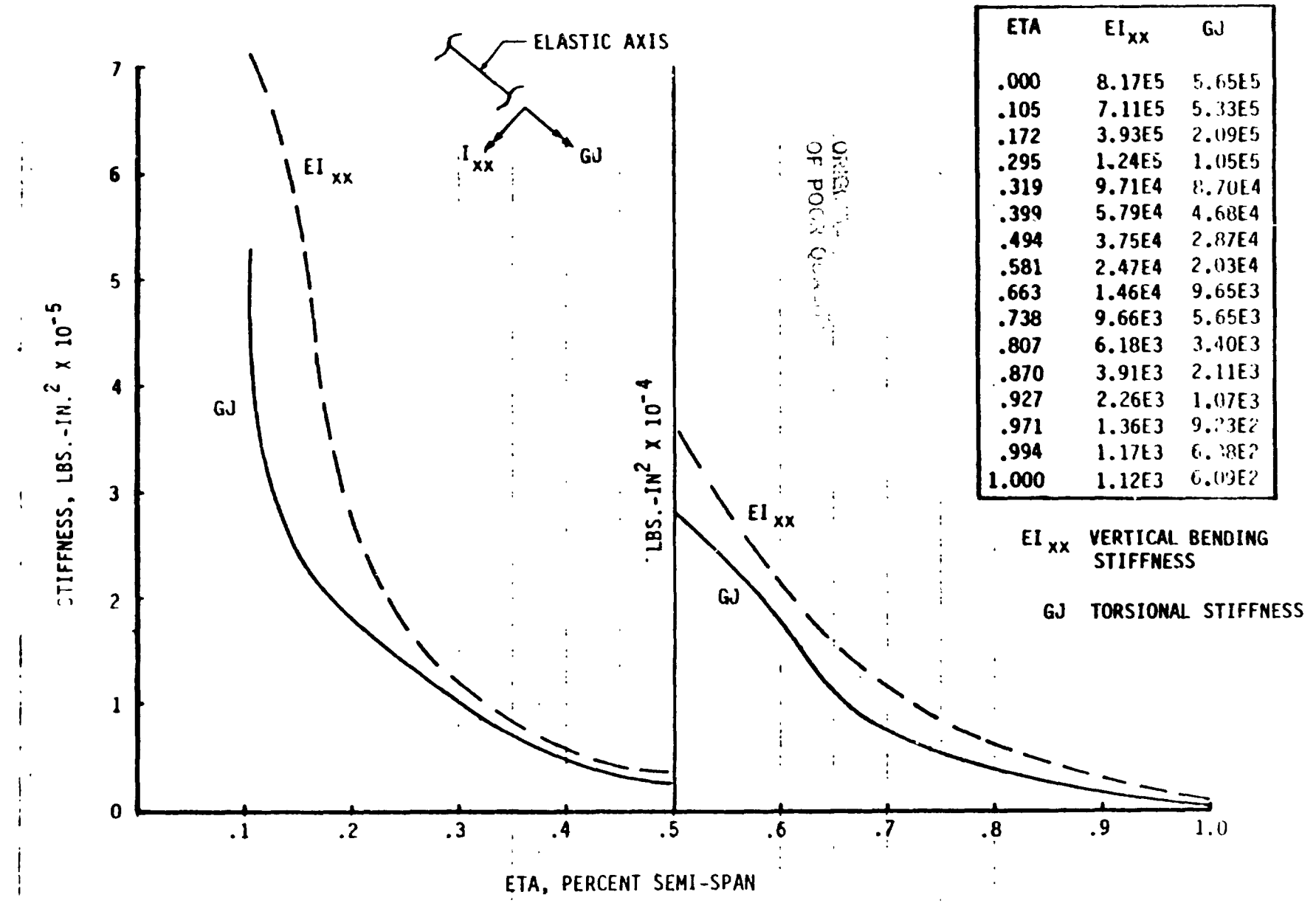

ETA	EI_{xx}	GJ
.000	8.17E5	5.65E5
.105	7.11E5	5.33E5
.172	3.93E5	2.09E5
.295	1.24E5	1.05E5
.319	9.71E4	8.70E4
.399	5.79E4	4.68E4
.494	3.75E4	2.87E4
.581	2.47E4	2.03E4
.663	1.46E4	9.65E3
.738	9.66E3	5.65E3
.807	6.18E3	3.40E3
.870	3.91E3	2.11E3
.927	2.26E3	1.07E3
.971	1.36E3	9.23E2
.994	1.17E3	6.38E2
1.000	1.12E3	6.09E2

EI_{xx} VERTICAL BENDING STIFFNESS

GJ TORSIONAL STIFFNESS

FIGURE A2 WINC SPANWISE STIFFNESS DISTRIBUTION ALONG ELASTIC AXIS

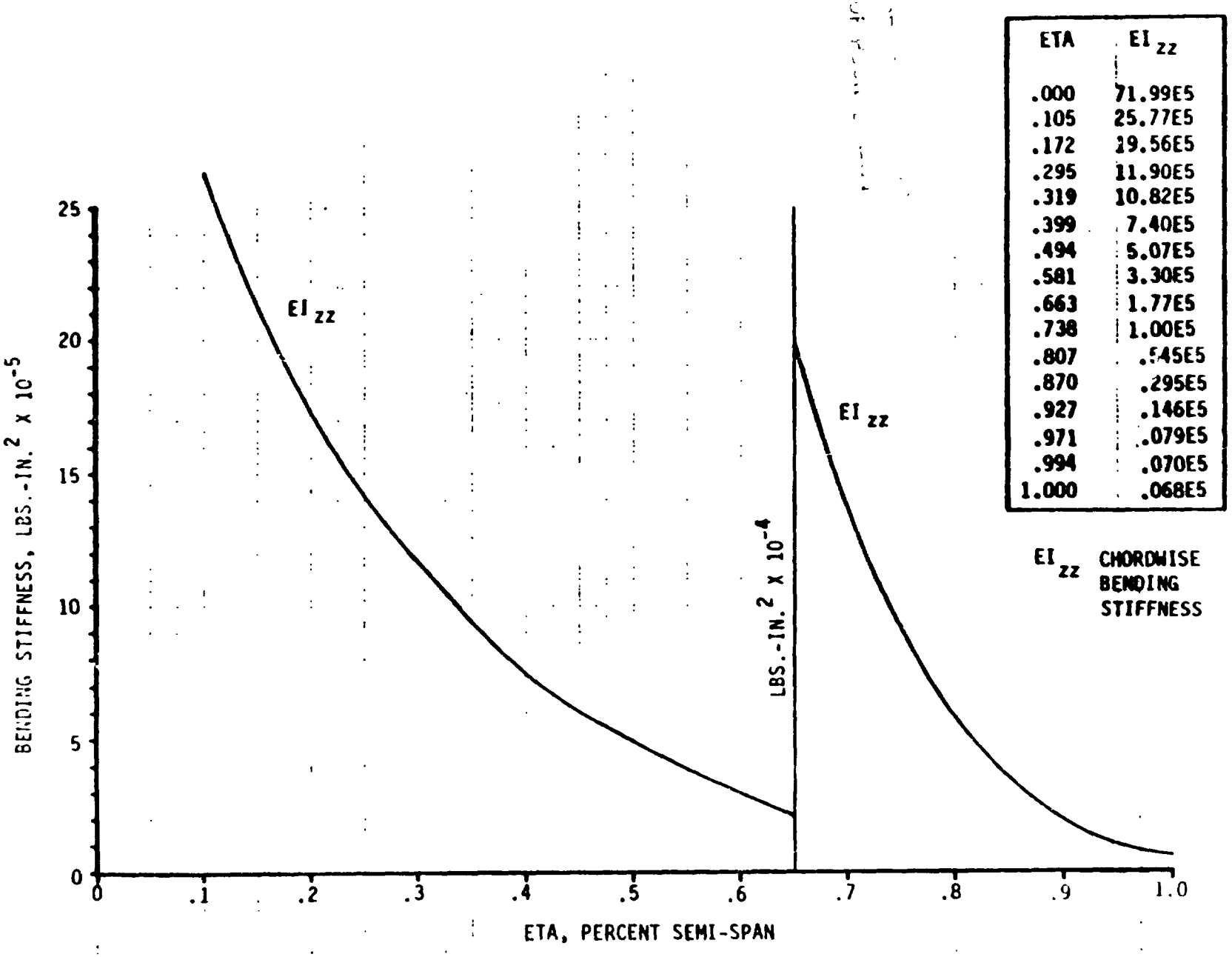

ETA	EI_{zz}
.000	71.99E5
.105	25.77E5
.172	19.56E5
.295	11.90E5
.319	10.82E5
.399	7.40E5
.494	5.07E5
.581	3.30E5
.663	1.77E5
.738	1.00E5
.807	.545E5
.870	.295E5
.927	.146E5
.971	.079E5
.994	.070E5
1.000	.068E5

EI_{zz} CHORDWISE BENDING STIFFNESS

FIGURE A2 CONT.

ATTACHMENT POINTS TO SPAR E.A.		X BODY STATION (Inches)	Y BODY BUTTLINE (Inches)	Z BODY WATERLINE (Inches)
CENTERLINE		13.444	0.0	9.558
SIDE OF BODY		13.444	5.845	9.558
WING SECTION	1	15.046	9.628	9.950
	2	18.313	16.438	10.662
	3	21.601	22.268	11.271
	4	24.580	27.550	11.823
	5	27.338	32.441	12.335
	6	29.911	37.003	12.812
	7	32.269	41.184	13.249
	8	34.446	45.044	13.652
	9	36.423	48.549	14.018
	10	38.140	51.549	14.337
	11	39.607	54.196	14.609
NACELLE		19.645	18.593	10.887
WINGLET		37.858	55.800	14.809

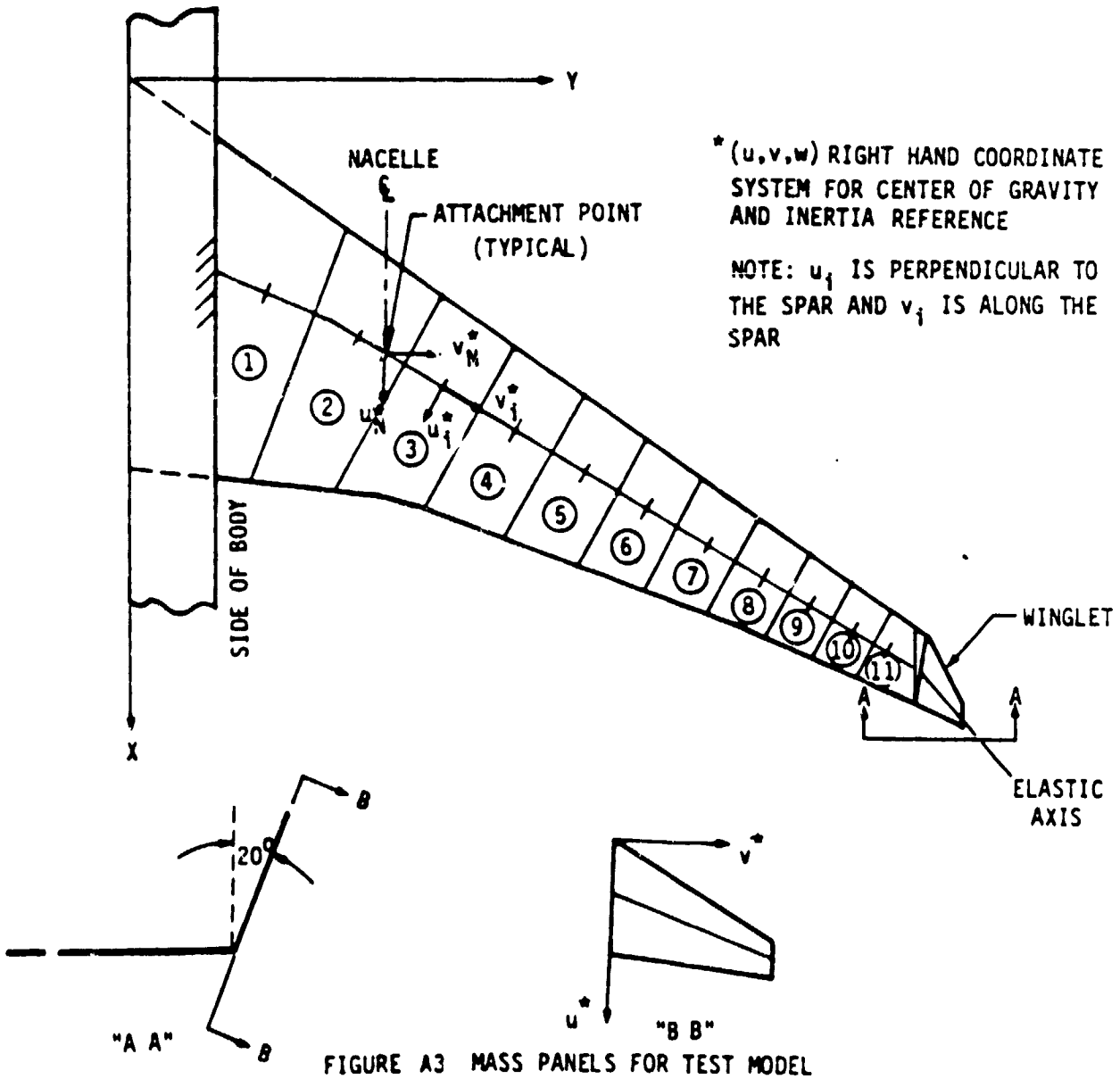

FIGURE A3 MASS PANELS FOR TEST MODEL

WING PANEL	W (LBS)	u (inches)	v (inches)	w (inches)	I_{uu} (lb-in^2)	I_{vv} (lb-in^2)	I_{ww} (lb-in^2)
1	2.6248	.058	-.686	-.251	23.8124	52.9615	74.6196
2	1.8712	1.746	-.158	.001	8.1056	35.1231	41.8933
3	.9023	.895	-.113	.085	3.3814	10.8500	13.9621
4	.8551	1.052	.524	.023	3.4742	8.2001	11.3327
5	.5052	-.090	-.058	.048	1.3723	3.0138	4.2647
6	.5319	.782	.563	.017	1.5685	3.0355	4.5407
7	.2767	-.339	-.023	.048	.4795	1.0191	1.4589
8	.2220	-.143	-.014	.044	.2957	.6733	.9472
9	.1983	-.050	.155	-.004	.2340	.4627	.6806
10	.1388	-.157	.022	.001	.1296	.2473	.3641
11	.0925	.155	.320	.004	.0828	.1120	.1616

	WEIGHT (LBS)	u (inches)	v (inches)	w (inches)	I_{uu} (lb-in^2)	I_{vv} (lb-in^2)	I_{ww} (lb-in^2)
WINGLET	.1025	3.60	2.71	0.0	.4025	.1493	.5516
MASS SIMULATOR	.1051	3.61	2.72	0.0	.0572	.0398	.0864

BRACKETS (INCL. 4 SCREWS AND REF. TO WING SECTION 11) FOR WINGLET AND SIMULATOR

CANT ANGLE	WEIGHT (LBS)	u (inches)	v (inches)	w (inches)
0°	.0206	0.00	1.91	0.
10°	.0257	0.00	1.91	0.
20°	.0288	0.00	1.91	0.

	WEIGHT (LBS)	u_N (inches)	v_N (inches)	w_N (inches)	$I_{u_Nu_N}$ (lb-in^2)	$I_{v_Nv_N}$ (lb-in^2)	$I_{w_Nw_N}$ (lb-in^2)
NACELLE	5.1903	-9.416	0.0	-4.108	14.3355	42.3143	39.6624
SPRING	.1655	-6.766	0.0	-0.898	.0100	.1350	.1253
CAGE	.4622	-2.886	0.0	-0.948	.0409	1.8050	1.7350
FARING	.0375	-8.766	0.0	-2.058	.1280	0.2780	0.3780

NOTE: 1. REFER TO FIGURE A3 FOR COORDINATE SYSTEM DEFINITION.
2. NO CONTRIBUTION TO GENERALIZED MASS FOR CANTILEVERED NACELLE MODES FROM SPRING, CAGE AND FARING.
3. ALL INERTIAS ARE ABOUT C.G.

FIGURE A4 MASS AND INERTIA PROPERTIES FOR
a) WING
b) WINGLET/SIMULATOR
c) NACELLE

WING PANEL	ITEM	WEIGHT (LBS)	u (inches)	v (inches)	w (inches)	I_{uu} (lb-in^2)	I_{vv} (lb-in^2)	I_{ww} (lb-in^2)
	100% AUXILIARY FUEL							
1		5.5098	-.76	-2.35	.58	6.9311	39.7134	42.3796
	100% MAIN FUEL							
1	R.H. ACTUAL	3.4972	-.93	1.87	.56	4.3650	20.4749	24.0578
2	R.H. ACTUAL	3.7785	.72	-.05	.48	18.8608	13.7770	32.2220
3	R.H. ACTUAL	2.6579	-.06	-.07	.36	8.6533	10.2835	18.8584
4	R.H. ACTUAL	1.8704	-.09	-.04	.31	5.2857	5.2866	10.5010
5	R.H. ACTUAL	1.3611	-.09	-.04	.25	3.2959	2.9136	6.1272
6	R.H. ACTUAL	.9698	-.08	-.02	.27	2.0711	1.4874	3.5045
7	R.H. ACTUAL	.5894	.04	-.16	.25	1.0228	.6643	1.6712
8	R.H. ACTUAL	.2256	04	-.25	.21	.4431	.1672	.6043
	75% MAIN FUEL							
1	R.H. ACTUAL	3.4972	-.93	1.87	.56	4.3650	20.4749	24.0578
2	R.H. ACTUAL	3.7785	.72	-.05	.48	18.8608	13.7770	32.2220
3	R.H. ACTUAL	2.5318	-.01	-.15	.35	7.8832	9.4998	17.1796
4	R.H. ACTUAL	1.1658	.14	-.42	.31	2.8934	3.2581	6.1142
5	R.H. ACTUAL	.2311	.51	-1.25	.20	.3585	.4650	.8159
	50% MAIN FUEL							
1	R.H. ACTUAL	3.4972	-.93	1.87	.56	4.3650	20.4749	24.0578
2	R.H. ACTUAL	3.1215	.91	-.34	.44	14.1900	10.7500	24.1240
3	R.H. ACTUAL	.9511	.59	-.74	.32	3.0124	3.3565	6.3946

NOTE: 1. REFER TO FIGURE A3 FOR COORDINATE SYSTEM DEFINITION

2. ALL INERTIAS ARE ABOUT C.G.

FIGURE A5 FUEL MASS AND INERTIA PROPERTIES

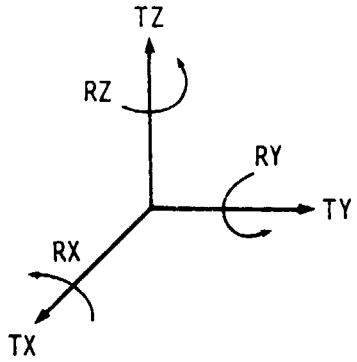

NO.	MODE	FREQ (HZ)	MODE SHAPE
1	NAC SIDE BNDG*	8.15	TY 1.0 RX .186 RZ -.139
2	NAC VERT BNDG*	8.79 (Soft)	
		10.60	TX -.72 TZ 1.0 RY .214
		11.37	
		11.72 (Nom)	
3	NAC ROLL*	17.96	TX -.07 TY -.05 TZ -.06
			RX 1.0 RY -.011 RZ -.478
4	WINGLET**	30.10	TZ 1.0 RX .032 RZ .017

*IN GLOBAL FRAME

**IN WINGLET REF FRAME (SEE FIG. A3)

FIGURE A6 CANTILEVERED NACELLE AND WINGLET FREQUENCIES AND MODE SHAPES

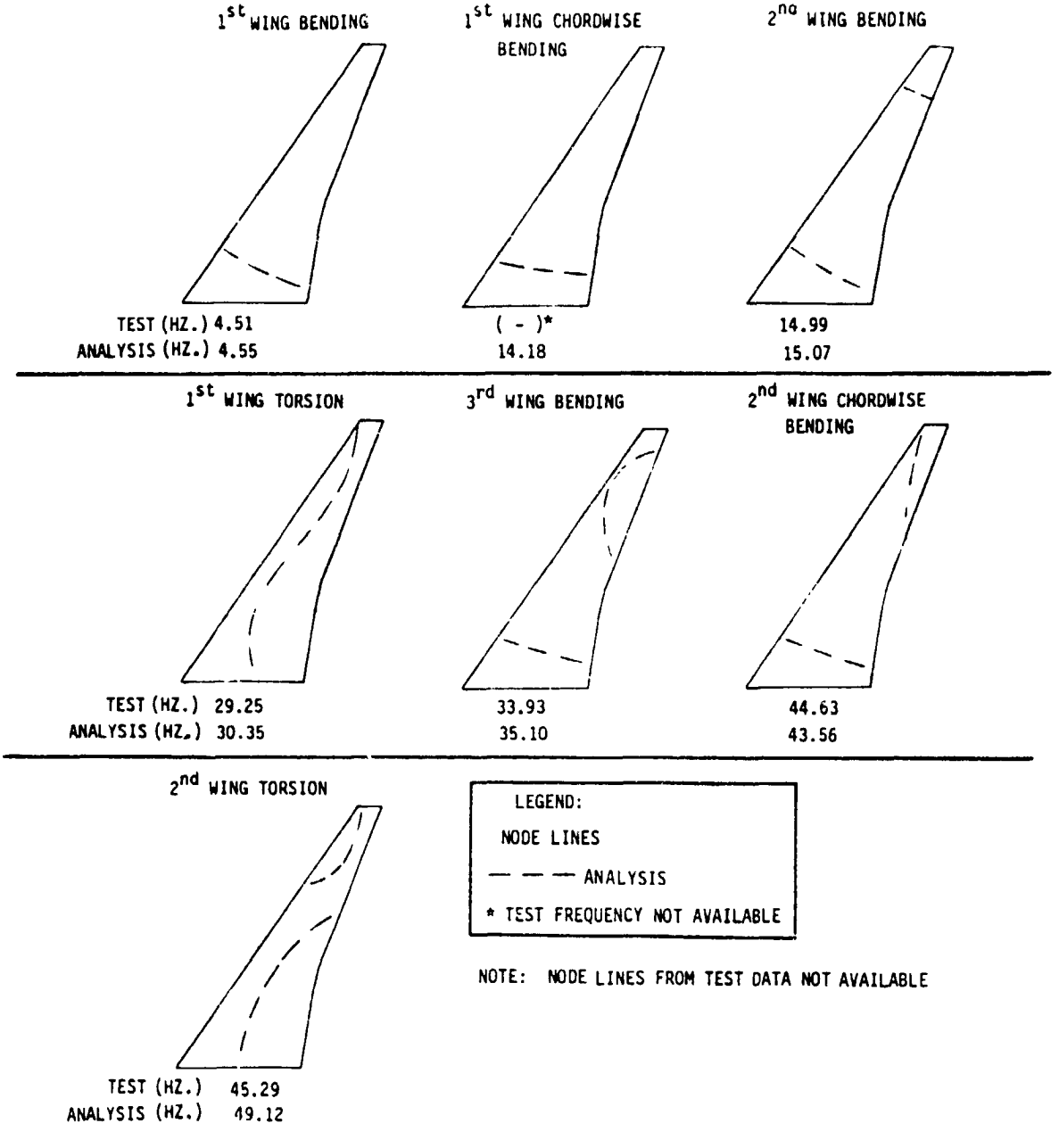

FIGURE A7 FREQUENCIES AND NODE LINES FOR
a) WINC (EMPTY), CALCULATED

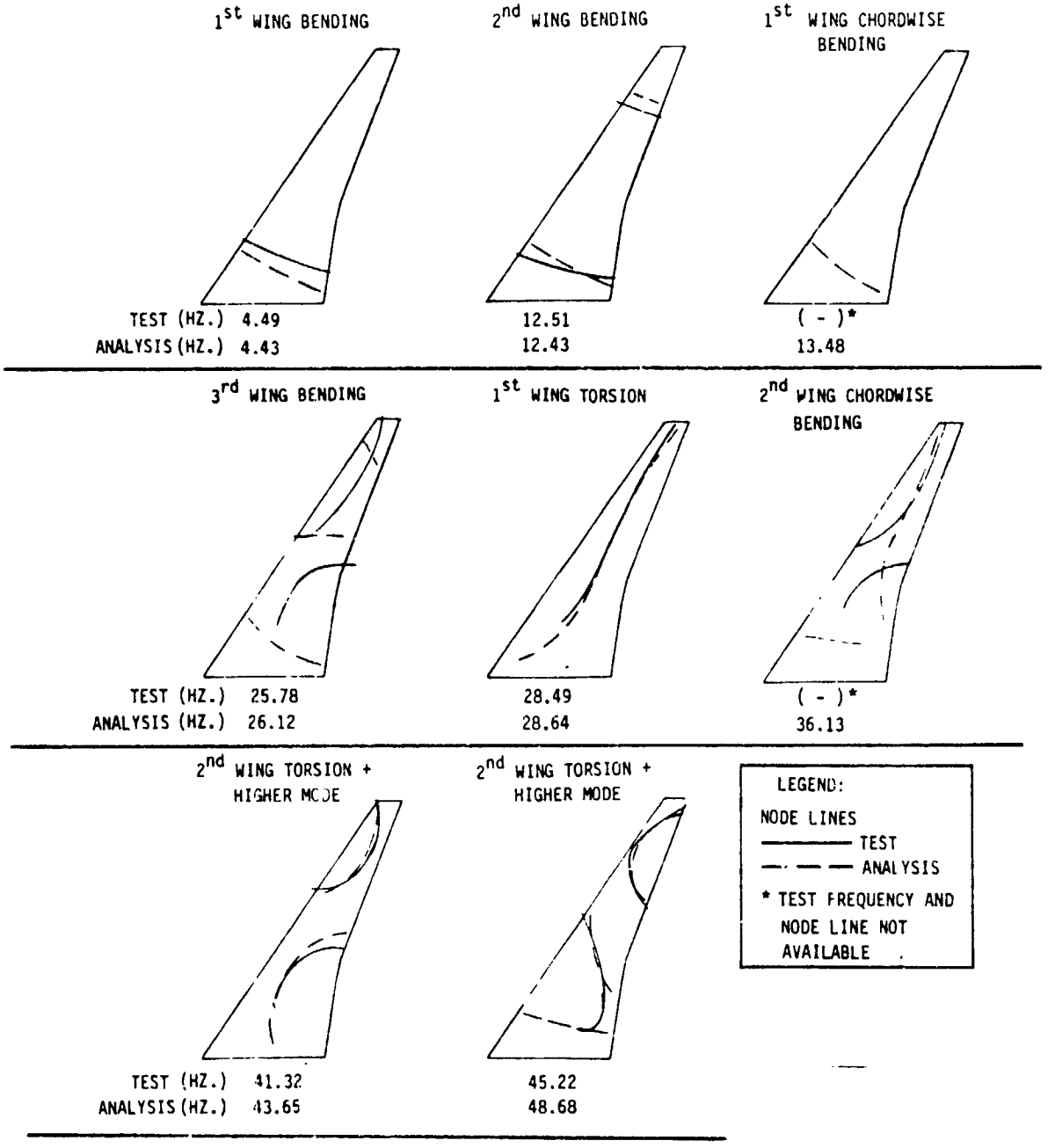

b) WING (75% FUEL), CALCULATED & MEASURED

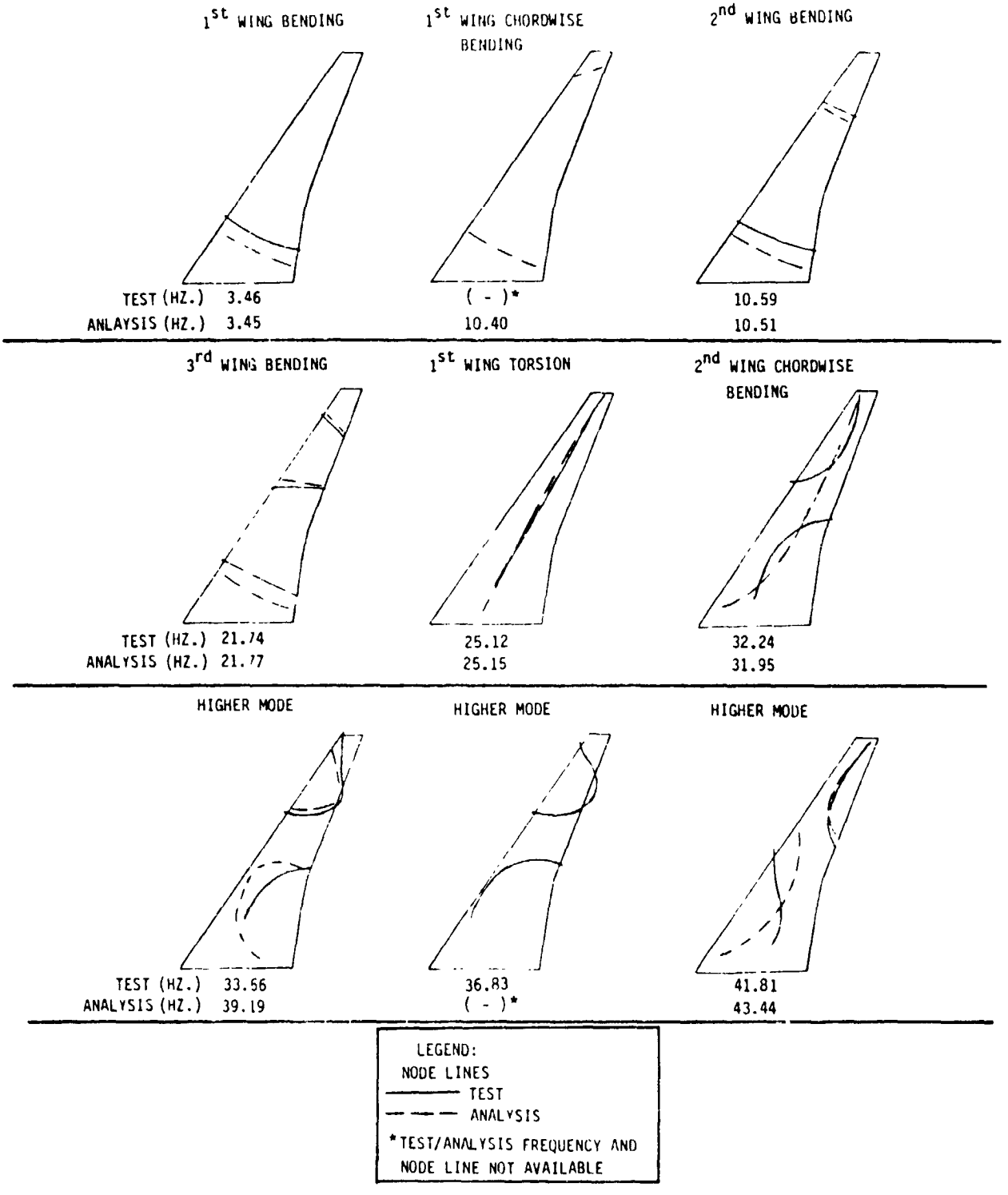

c) WINC (100% FUEL), CALCULATED & MEASURED

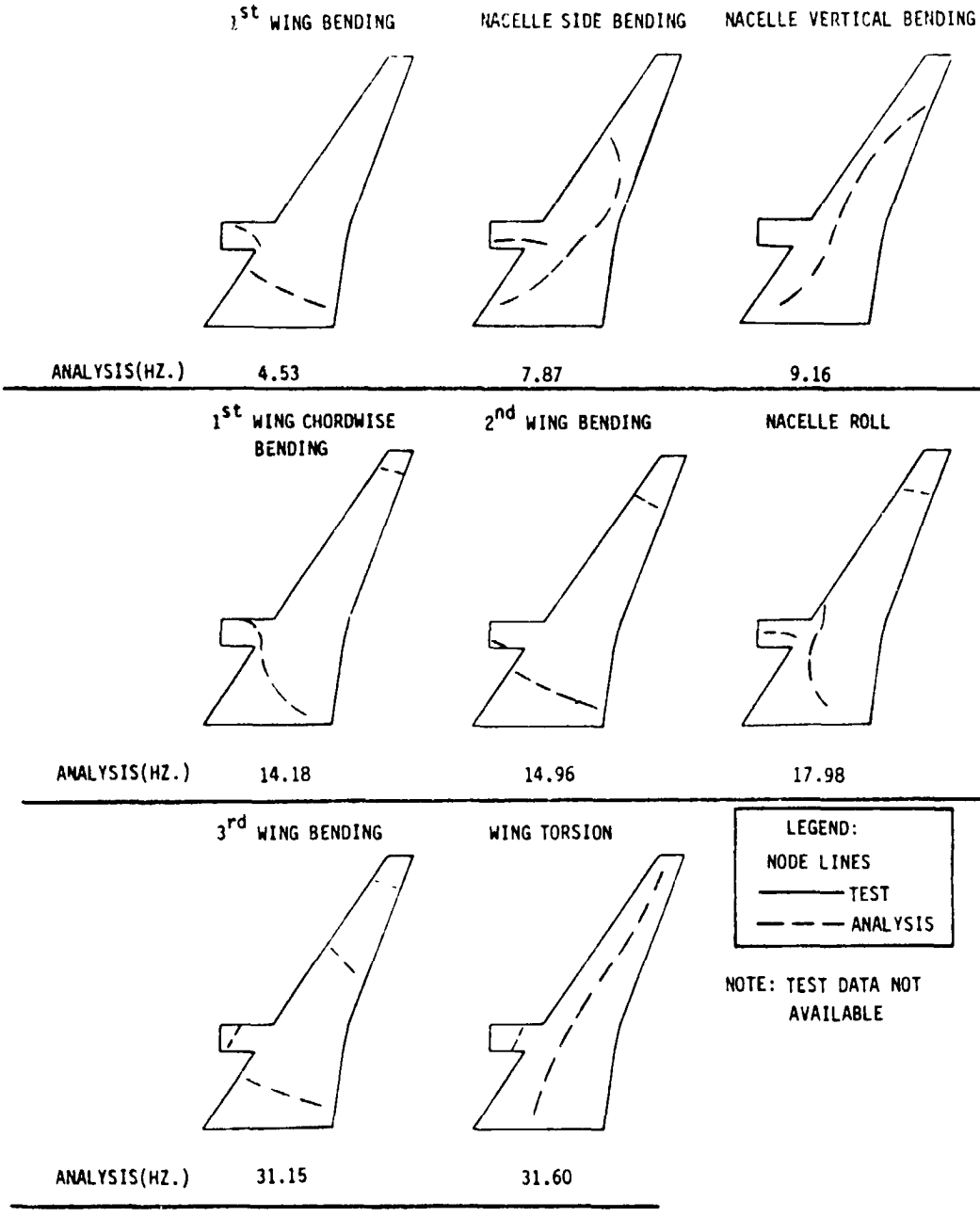

d) WING (EMPTY) - NACELLE (NOMINAL), CALCULATED

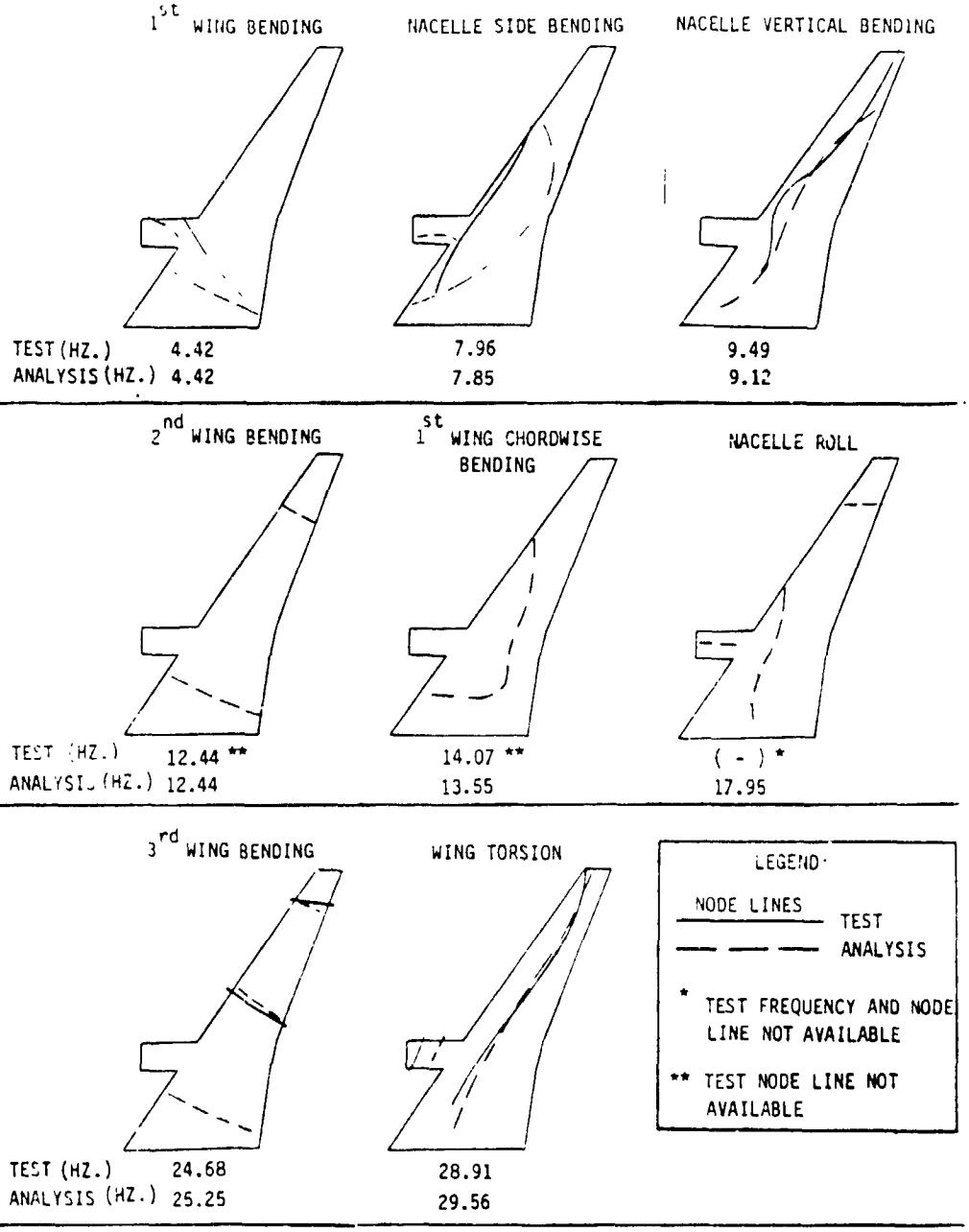

e) WING (75% FUEL) - NACELLE (NOMINAL), CALCULATED & MEASURED

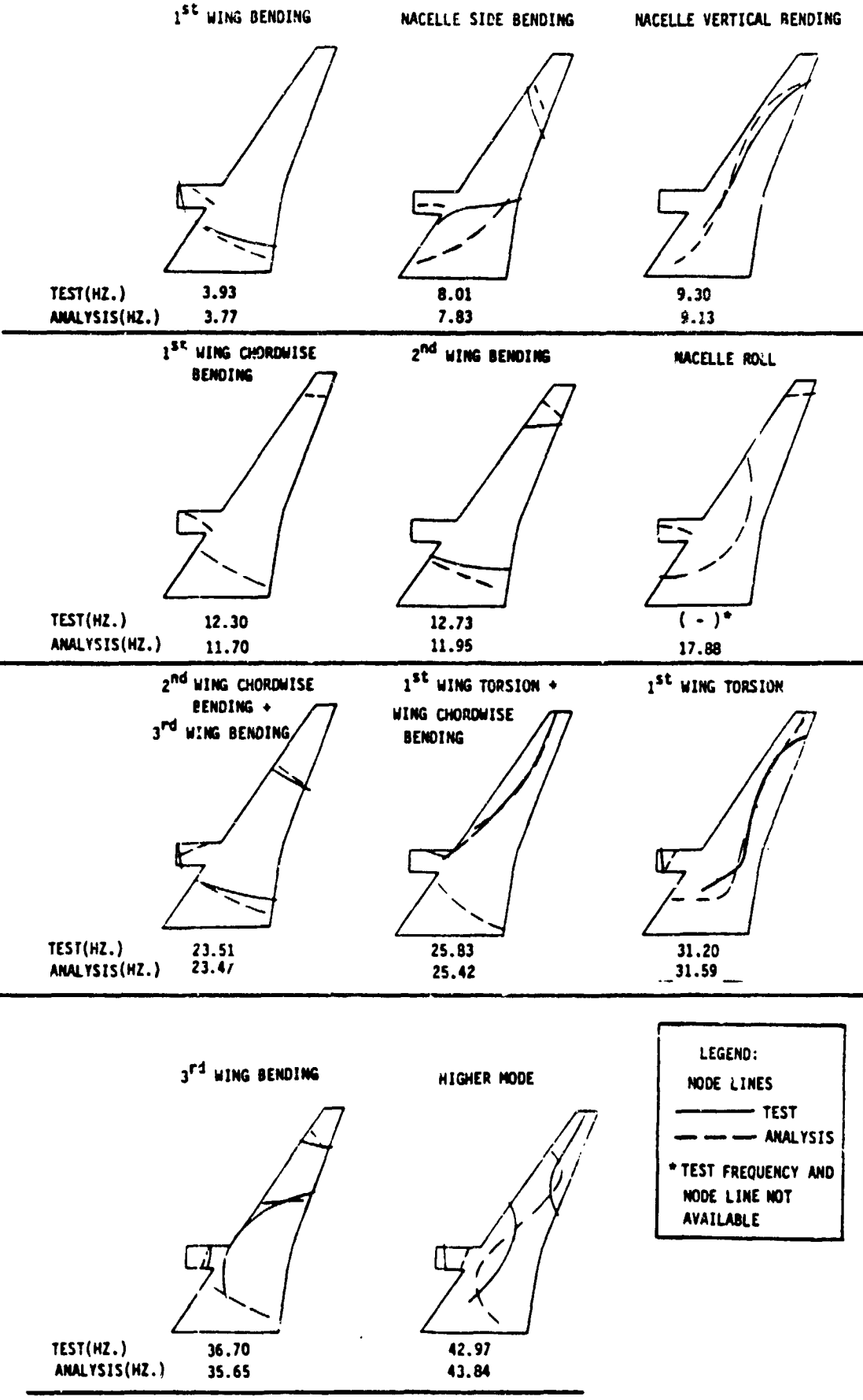

f) WING (EMPTY) - NACELLE (NOMINAL) - SIMULATOR (20 DEG)
CALCULATED & MEASURED

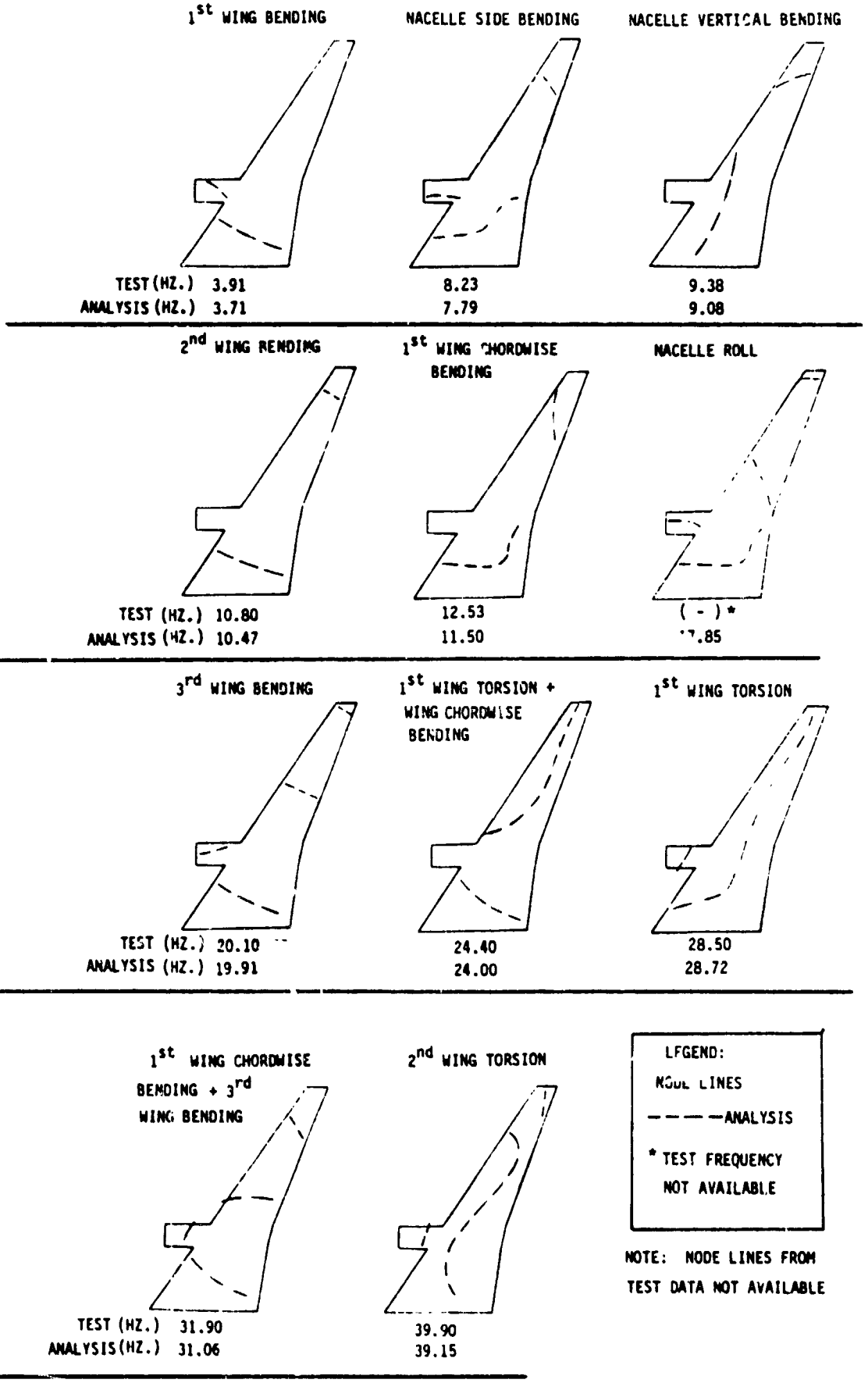

g) WING (75% FUEL) - NACELLE (NOMINAL) - SIMULATOR (20 DEC), CALCULATED

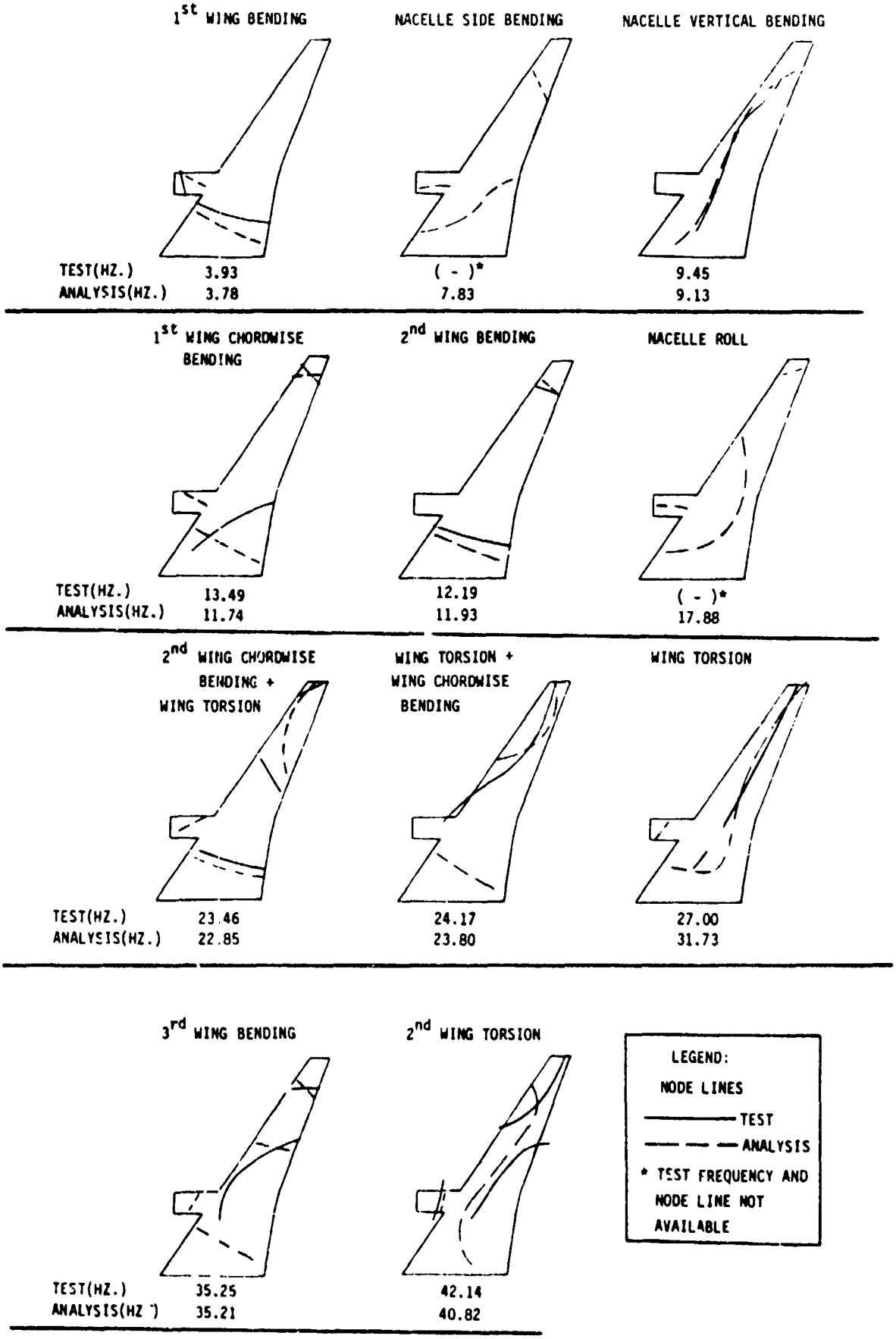

h) WING (EMPTY) - NACELLE (NOMINAL) - WINGLET (20 DEC)
CALCULATED & MEASURED

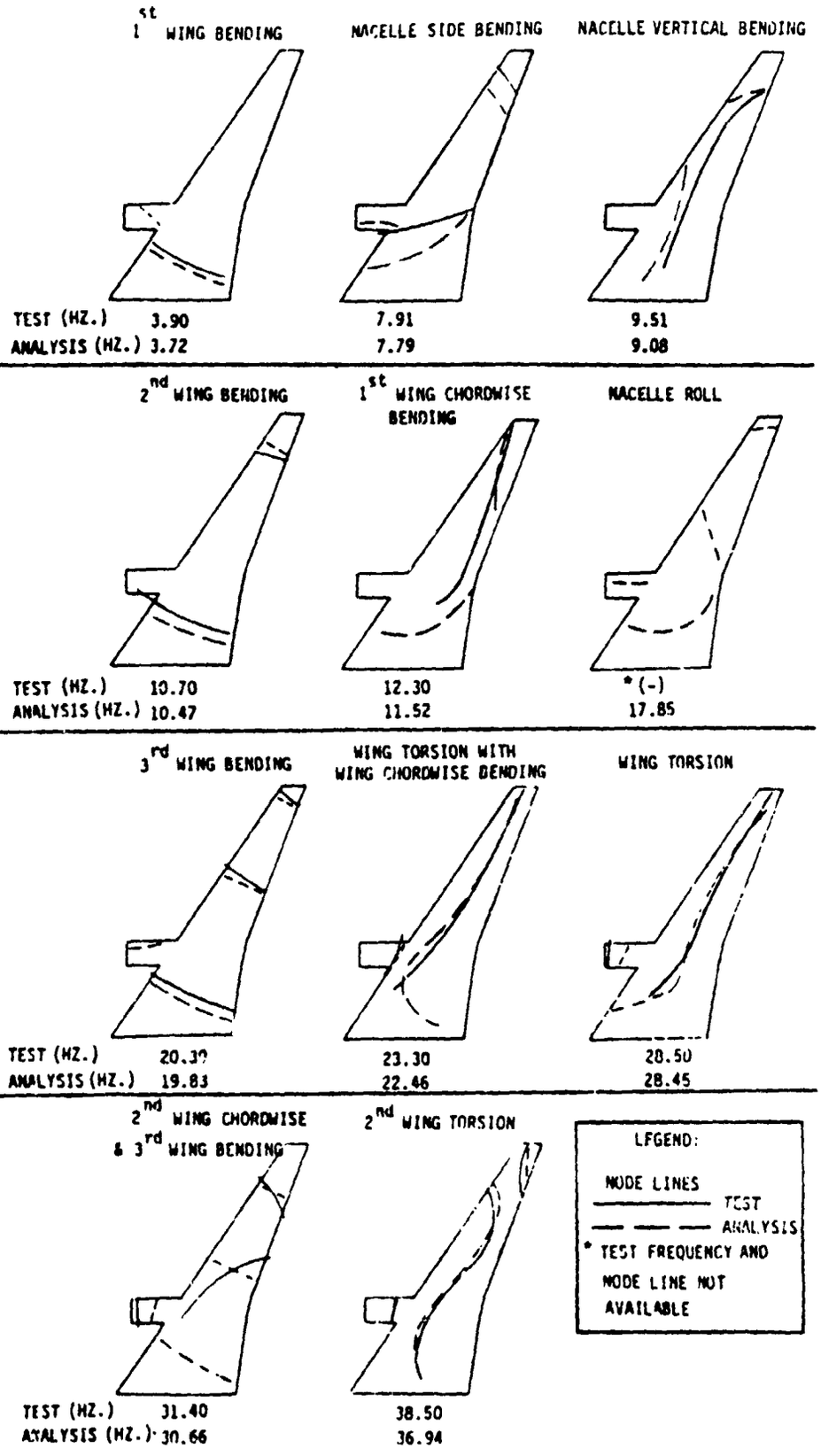

1) WING (75% FUEL) - NACELLE (NOMINAL) - WINGLET (20 DEG)
CALCULATED & MEASURED